MATHEMATICS OF COMPUTATION
Volume 88, Number 317, May 2019, Pages 1121–1153
https://doi.org/10.1090/mcom/3365
Article electronically published on June 19, 2018

UPWIND DISCONTINUOUS GALERKIN SPACE DISCRETIZATION AND LOCALLY IMPLICIT TIME INTEGRATION FOR LINEAR MAXWELL'S EQUATIONS

MARLIS HOCHBRUCK AND ANDREAS STURM

Abstract. This paper is dedicated to the full discretization of linear Maxwell's equations, where the space discretization is carried out with a discontinuous Galerkin (dG) method on a locally refined spatial grid. For such problems explicit time integrators are inefficient due to their strict CFL condition stemming from the fine grid elements. In the last few years this issue of so-called grid-induced stiffness was successfully tackled with locally implicit time integrators. So far, these methods are limited to unstabilized (central fluxes) dG methods. However, stabilized (upwind fluxes) dG schemes provide many benefits and thus are a popular choice in applications. In this paper we construct a new variant of a locally implicit time integrator using an upwind fluxes dG discretization on the coarse part of the grid. The construction is based on a rigorous error analysis which shows that the stabilization operators have to be split differently than the Maxwell operator. Moreover, our earlier analysis of a central fluxes locally implicit method based on semigroup theory applies but does not yield optimal convergence rates. In this paper we rigorously prove the stability and provide error bounds of the new method with optimal rates in space and time by means of an energy technique for a suitably defined modified error.

1. Introduction

We consider the full discretization of Maxwell's equations following the method of lines technique. In this approach the continuous problem is first discretized in space and subsequently integrated in time. For the space discretization discontinuous Galerkin (dG) methods are a popular choice since they exhibit many attractive features; cf. [8,20]. For example, they easily allow one to handle complex geometries and composite media by using unstructured, possibly locally refined meshes. In addition, dG methods lead to block diagonal mass matrices which in combination with an explicit time integrator result in a fully explicit scheme.

However, the spatial discretization of Maxwell's equations results in a system of stiff ODEs. For such problems explicit time integrators suffer from severe stability issues. In fact, in order to guarantee stability, the time step of these methods is subject to a strong limitation (CFL condition). For Maxwell's equations we have to ensure that the time step satisfies $\tau \lesssim h_{\min}$, where $h_{\min}$ denotes the smallest

Received by the editor May 26, 2017, and, in revised form, December 29, 2017, and January 25, 2018.

2010 *Mathematics Subject Classification.* Primary 65M12, 65M15; Secondary 65M60, 65J10.

Key words and phrases. Locally implicit methods, time integration, upwind fluxes discontinuous Galerkin finite elements, error analysis, energy techniques, Maxwell's equations.

We gratefully acknowledge financial support by the Deutsche Forschungsgemeinschaft (DFG) through CRC 1173.

diameter of the elements in the spatial grid. Because of this limitation explicit time integrators perform poorly when the space discretization is carried out on a locally refined grid, i.e., a grid that consists of only a few fine elements with a very small diameter but a large number of coarse elements. This occurs in a plurality of applications, e.g., in nanophotonics [3], numerical dosimetry [6] or seismology [13], where fine mesh elements are needed to capture a complex geometry. Even on nice geometries locally refined meshes can be advantageous, e.g., if the exact solution of the problem locally lacks regularity (corner singularities). For wave equations it was shown in [28] that the solution remains smooth in neighborhoods separated from the corner. Moreover, it was shown that graded meshes yield quasi-optimal convergence rates of the finite element discretization. In all these cases a fixed spatial mesh can be employed but the few fine elements lead to a strong CFL condition (grid-induced stiffness) which enforces a small time step size. The large number of tiny time steps yields an approximation with temporal error being much smaller than the space discretization error, since the dominant part of the latter stems from the coarse elements. This renders explicit time integrators inefficient. Applying suitable implicit time integrators eliminates this restriction. However, in each time step, implicit methods require the solution of a linear system of equations involving all degrees of freedom in the spatial grid. A single time step with an implicit scheme is significantly more expensive than for explicit methods. For large 3d problems implicit methods might even be unfeasible.

As a remedy, local time stepping methods [1, 4, 9, 10, 15, 17, 18, 21] have been proposed. These schemes use a smaller time step to integrate the fine mesh elements in order to relax the CFL condition. However, the stability of these schemes is still an open problem. The recent analysis in [16] requires a CFL condition depending on the fine mesh elements and it is still an open problem to prove that local time stepping methods are stable under a CFL condition depending on the coarse mesh only. Another approach consists in combining explicit and implicit time integrators to so-called locally implicit methods. These methods apply an implicit time integrator to the fine mesh elements—thus avoiding a restrictive CFL condition—while retaining an explicit time integration for the coarse mesh elements. For Maxwell's equations they were initially proposed in [30, 32], analyzed in [5, 12, 24, 27] and extended to dispersive media in [6, 7]. So far, these methods are only considered for unstabilized spatial discretizations of Maxwell's equations, the so-called central fluxes dG discretizations. However, a stabilized dG discretization (upwind fluxes dG method) provides many benefits such as an improved stability behavior and a higher spatial convergence rate. The purpose of this paper is to construct a new locally implicit time integrator based on an upwind fluxes dG space discretization comprising the explicit Verlet (or leap frog) method and the implicit Crank–Nicolson method.

Although some ideas (and also the notation) are taken from [24], the extension of the central fluxes method to upwind fluxes is by far not obvious. It is based on a rigorous error analysis which shows that the splitting of the stabilization operators has to be done differently than the splitting of the Maxwell operator presented in [24]. Moreover, it turns out that the techniques developed in [24] are not appropriate to show the improved stability and convergence of the full discretization of the locally implicit upwind fluxes scheme. In fact, in order to reveal the benefits of an upwind fluxes dG method our analysis is based on an energy technique as presented in [22] for fully implicit Runge–Kutta discretizations

of the linear Maxwell's equations. This technique renders the analysis far more involved compared to the discrete variation-of-constants techniques we used in [24]. For instance, the analysis involves additional defects arising from the incorporation of the stabilization operators and has to be applied to a carefully chosen modified error instead of the error itself. Last, we point out that as a byproduct we obtain a stability and error analysis for an upwind fluxes Verlet-type fully explicit time integrator.

Our main contributions are as follows: We show that this novel method retains the efficiency of the underlying locally implicit time integrator while gaining the benefits of an upwind fluxes space discretization. In particular, we provide a rigorous stability and error analysis of the full discretization and prove that:

(a) the method is stable under a CFL condition that solely depends on the coarse elements in the spatial grid, and
(b) the full discretization error is of order two in the time step and of order $k + 1/2$ and k in the space discretization parameter in the coarse elements and in the fine elements, respectively, if we use polynomials of order k (and in a few elements of order $k + 1$).

We organize our paper as follows. In Section 2 we present the main ideas of the construction and the results of the locally implicit method which we elaborate in the remaining paper. We begin in Section 3 with a short overview of the continuous linear Maxwell's equations and their well-posedness. Section 4 is dedicated to the spatial discretization of Maxwell's equations. In particular, we decompose the spatial mesh into explicitly and implicitly treated elements. On this basis we construct split discrete operators that we use in Section 5 to derive our locally implicit time integrator. Subsequently, we examine the stability behavior of the method and carry out its error analysis. Combining these results leads to our main result which is given in short form in Theorem 2.1 and with all details in Theorem 5.10. Last, in Section 6 we present numerical experiments verifying our theoretical results. A careful study of the efficiency of the locally implicit method for large problems, in particular, in comparison with local time stepping methods, is ongoing work and will be presented elsewhere.

2. Locally implicit scheme

In this section we present the main ideas of this paper and elaborate the details in the subsequent sections.

Let $\Omega \subset \mathbb{R}^d$, $d = 1, 2, 3$, be an open, bounded Lipschitz domain and let $T > 0$ be a finite time. We consider the linear Maxwell's equations in a composite medium with permeability $\mu : \Omega \to \mathbb{R}$, permittivity $\varepsilon : \Omega \to \mathbb{R}$ and a perfect conduction boundary,

$$\begin{aligned} \mu \partial_t \mathbf{H} &= -\operatorname{curl} \mathbf{E}, && (0,T) \times \Omega, \\ \varepsilon \partial_t \mathbf{E} &= \operatorname{curl} \mathbf{H} - \mathbf{J}, && (0,T) \times \Omega, \\ \mathbf{H}(0) &= \mathbf{H}^0, \quad \mathbf{E}(0) = \mathbf{E}^0, && \Omega, \\ n \times \mathbf{E} &= 0, && (0,T) \times \partial\Omega. \end{aligned} \tag{2.1}$$

Here, the unknowns $\mathbf{H}, \mathbf{E} : (0,T) \times \Omega \to \mathbb{R}^d$ are the magnetic and electric field, respectively, and $\mathbf{J} : (0,T) \times \Omega \to \mathbb{R}^d$ is a given electric current density. Furthermore,

n denotes the unit outer normal vector of the domain Ω. It is well known that the solution $(\mathbf{H}(t), \mathbf{E}(t))$ of (2.1) preserves the electromagnetic energy

$$\mathcal{E}(\mathbf{H}, \mathbf{E}) = \frac{1}{2}\Big(\|\mathbf{H}\|_\mu^2 + \|\mathbf{E}\|_\varepsilon^2\Big), \tag{2.2}$$

i.e., for vanishing source term $\mathbf{J}(t) \equiv 0$ we have $\mathcal{E}\big(\mathbf{H}(t), \mathbf{E}(t)\big) = \mathcal{E}\big(\mathbf{H}^0, \mathbf{E}^0\big)$ for $t \geq 0$.

We discretize (2.1) in space using a dG method. This results in the semidiscrete problem,

$$\begin{aligned} \partial_t \mathbf{H}_h(t) &= -\boldsymbol{\mathcal{C}}_{\mathbf{E}} \mathbf{E}_h(t) - \alpha \boldsymbol{\mathcal{S}}_{\mathbf{H}} \mathbf{H}_h(t), && (0,T), \\ \partial_t \mathbf{E}_h(t) &= \boldsymbol{\mathcal{C}}_{\mathbf{H}} \mathbf{H}_h(t) - \alpha \boldsymbol{\mathcal{S}}_{\mathbf{E}} \mathbf{E}_h(t) - \mathbf{J}_h(t), && (0,T), \\ \mathbf{H}_h(0) &= \mathbf{H}_h^0, \quad \mathbf{E}_h(0) = \mathbf{E}_h^0, \end{aligned} \tag{2.3}$$

where $\boldsymbol{\mathcal{C}}_{\mathbf{E}}$ and $\boldsymbol{\mathcal{C}}_{\mathbf{H}}$ denote the spatially discretized curl-operators, $\boldsymbol{\mathcal{S}}_{\mathbf{H}}$ and $\boldsymbol{\mathcal{S}}_{\mathbf{E}}$ are stabilization operators and $\alpha \in [0,1]$ is the parameter controlling the stabilization. The boundary condition $(n \times \mathbf{E}_h(t))|_{\partial\Omega} = 0$ is weakly enforced within the definition of $\boldsymbol{\mathcal{C}}_{\mathbf{E}}$; see (4.8b) below.

For $\alpha = 0$ our dG method is not stabilized, which renders it a central fluxes dG discretization. Such a method is convergent with order k, if we employ polynomials of degree k in our spatial discretization. Similar to the continuous Maxwell's equations the semidiscrete Maxwell's equations (2.3) preserve the electromagnetic energy $\mathcal{E}(\mathbf{H}_h, \mathbf{E}_h)$ in the case of a central fluxes dG discretization. On the other hand, if we choose $\alpha \in (0,1]$, we obtain a stabilized dG space discretization, which is usually referred to as an upwind fluxes dG method. In contrary to the central fluxes method such a space discretization is dissipative, i.e., it decreases the electromagnetic energy $\mathcal{E}(\mathbf{H}_h, \mathbf{E}_h)$ if time evolves. This dissipative behavior is beneficial in view of enhanced stability and a higher convergence rate $k + 1/2$ of the upwind fluxes method.

In this paper we consider the case where the space discretization is carried out with a locally refined mesh $\mathcal{T}_h$, i.e., a mesh that consists of mostly coarse elements and a few fine elements. We collect the coarse elements in $\mathcal{T}_{h,c}$ and the fine elements in $\mathcal{T}_{h,f}$ so that

$$\mathcal{T}_h = \mathcal{T}_{h,c} \,\dot\cup\, \mathcal{T}_{h,f}, \qquad \operatorname{card}(\mathcal{T}_{h,f}) \ll \operatorname{card}(\mathcal{T}_{h,c}). \tag{2.4}$$

In order to obtain a fully discrete numerical scheme, the semidiscrete problem (2.3) has further to be integrated in time. If the space discretization relies on a locally refined grid, locally implicit time integrators are an appealing choice. For these schemes we decompose the mesh $\mathcal{T}_h$ subject to

$$\mathcal{T}_h = \mathcal{T}_{h,e} \,\dot\cup\, \mathcal{T}_{h,i}, \qquad \mathcal{T}_{h,f} \subset \mathcal{T}_{h,i}, \quad \mathcal{T}_{h,e} \subset \mathcal{T}_{h,c},$$

where $\mathcal{T}_{h,e}$ contains the explicitly treated elements and $\mathcal{T}_{h,i}$ contains the implicitly treated ones. Based on this decomposition we constructed in [24] explicit and implicit discrete curl-operators $\boldsymbol{\mathcal{C}}_{\mathbf{H}}^e$ and $\boldsymbol{\mathcal{C}}_{\mathbf{H}}^i$, respectively, which enabled us to merge the explicit Verlet (or leap frog) method and the implicit Crank–Nicolson method following an idea of [32] to a locally implicit time integrator. The resulting locally implicit scheme agrees with the scheme (2.5) below with $\alpha = 0$. Here, τ denotes the time step size. However, this method could not treat the stabilization operators $\boldsymbol{\mathcal{S}}_{\mathbf{H}}$ and $\boldsymbol{\mathcal{S}}_{\mathbf{E}}$ from (2.3). We extend it with the following two ideas: First, in order to inherit the efficiency of the central fluxes locally implicit scheme, we integrate

the stabilization operators explicitely (i.e., we do not include them into the Crank–Nicolson scheme). Second, we retain a CFL condition independent of the fine part of the mesh by stabilizing only on the explicitly treated elements. We realize these ideas by using explicit stabilization operators $\boldsymbol{\mathcal{S}}^e_{\mathbf{H}}$, $\boldsymbol{\mathcal{S}}^e_{\mathbf{E}}$ instead of the full stabilization operators $\boldsymbol{\mathcal{S}}_{\mathbf{H}}$, $\boldsymbol{\mathcal{S}}_{\mathbf{E}}$. This results in the following locally implicit scheme:

$$\mathbf{H}_h^{n+1/2} - \mathbf{H}_h^n = -\frac{\tau}{2}\boldsymbol{\mathcal{C}}_{\mathbf{E}}\mathbf{E}_h^n - \frac{\tau}{2}\alpha\boldsymbol{\mathcal{S}}^e_{\mathbf{H}}\mathbf{H}_h^n, \tag{2.5a}$$

$$\begin{aligned}\mathbf{E}_h^{n+1} - \mathbf{E}_h^n =& \tau\boldsymbol{\mathcal{C}}^e_{\mathbf{H}}\mathbf{H}_h^{n+1/2} + \frac{\tau}{2}\boldsymbol{\mathcal{C}}^i_{\mathbf{H}}\big(\mathbf{H}_h^{n+1} + \mathbf{H}_h^n\big) - \tau\alpha\boldsymbol{\mathcal{S}}^e_{\mathbf{E}}\mathbf{E}_h^n \\ &- \frac{\tau}{2}\big(\mathbf{J}_h^{n+1} + \mathbf{J}_h^n\big),\end{aligned} \tag{2.5b}$$

$$\mathbf{H}_h^{n+1} - \mathbf{H}_h^{n+1/2} = -\frac{\tau}{2}\boldsymbol{\mathcal{C}}_{\mathbf{E}}\mathbf{E}_h^{n+1} - \frac{\tau}{2}\alpha\boldsymbol{\mathcal{S}}^e_{\mathbf{H}}\mathbf{H}_h^n. \tag{2.5c}$$

The details of the construction of the stabilization operators will be given below.

Our main result is the following error bound for the fully discrete scheme.

Theorem 2.1. *Let the solution* $(\mathbf{H}, \mathbf{E})$ *of* (2.1) *be sufficiently smooth. Then, for* $\alpha \in (0, 1]$ *the error of the numerical scheme* (2.5) *satisfies*

$$\|(\mathbf{H}_h^n, \mathbf{E}_h^n) - (\mathbf{H}(t_n), \mathbf{E}(t_n))\| \le CT\big(\tau^2 + \max_{K\in\mathcal{T}_{h,e}} h_K^{k+1/2} + \max_{K\in\mathcal{T}_{h,i}} h_K^k\big),$$

if τ *satisfies a CFL condition depending on the coarse mesh only.*

The precise formulation of this theorem including the regularity assumptions together with its proof is given in Theorem 5.10 below. Here, we only stress that the technique to prove these bounds cannot be transfered directly from [24] and is considerably more involved. Last, let us mention that dG methods easily allow one to choose the polynomial degree differently in every mesh element. As we will show below by using polynomials of order $k+1$ for a small set of elements (the coarse neighbors of the fine elements) we can obtain the more favorable bound

$$\|(\mathbf{H}_h^n, \mathbf{E}_h^n) - (\mathbf{H}(t_n), \mathbf{E}(t_n))\| \le CT\big(\tau^2 + \max_{K\in\mathcal{T}_{h,c}} h_K^{k+1/2} + \max_{K\in\mathcal{T}_{h,f}} h_K^k\big),$$

which shows convergence of order $k+1/2$ on all coarse elements.

3. Analytic setting

We begin by introducing some notation. For a set $K \subset \Omega$ and vector fields $\mathbf{U}, \widehat{\mathbf{U}}, \mathbf{V}, \widehat{\mathbf{V}}$ (in $\mathbb{R}^3$) we denote the $L^2(K)$-inner product and the $L^2(F)$-inner product, $F \subset \partial K$, by

$$\big(\mathbf{U}, \widehat{\mathbf{U}}\big)_K = \int_K \mathbf{U}\cdot\widehat{\mathbf{U}}\,dx, \qquad \big(\mathbf{U}, \widehat{\mathbf{U}}\big)_F = \int_F \mathbf{U}|_F\cdot\widehat{\mathbf{U}}|_F\,d\sigma,$$

respectively. For $\mathbf{u} = (\mathbf{U}, \mathbf{V})$, $\widehat{\mathbf{u}} = (\widehat{\mathbf{U}}, \widehat{\mathbf{V}})$, and uniformly positive weight functions $\omega_1, \omega_2 : \Omega \to \mathbb{R}_{>0}$ we write the weighted inner products as

$$\big(\mathbf{U}, \widehat{\mathbf{U}}\big)_{\omega_1,K} = \big(\omega_1\mathbf{U}, \widehat{\mathbf{U}}\big)_K, \qquad \big(\mathbf{u}, \widehat{\mathbf{u}}\big)_{\omega_1\times\omega_2,K} = \big(\mathbf{U}, \widehat{\mathbf{U}}\big)_{\omega_1,K} + \big(\mathbf{V}, \widehat{\mathbf{V}}\big)_{\omega_2,K}. \tag{3.1}$$

By $\|\cdot\|_{\omega_1}$ and $\|\cdot\|_{\omega_1\times\omega_2}$ we denote the corresponding norms. We abbreviate $\big(\cdot,\cdot\big) = \big(\cdot,\cdot\big)_\Omega$ and $\|\cdot\| = \|\cdot\|_\Omega$ and analogously for the weighted inner products and norms.

Next, we cast Maxwell's equations (2.1) into a more compact form. In fact, by introducing the combined field $\mathbf{u} = (\mathbf{H}, \mathbf{E})$ we can write (2.1) equivalently as

$$\partial_t \mathbf{u}(t) = \mathcal{C}\mathbf{u}(t) + \mathbf{j}(t), \qquad \mathbf{u}(0) = \mathbf{u}^0, \tag{3.2}$$

where the source term is $\mathbf{j} = (0, -\varepsilon^{-1}\mathbf{J})$ and where $\mathcal{C}$ is the so-called Maxwell operator given by

$$\mathcal{C} : D(\mathcal{C}) \to L^2(\Omega)^6, \qquad \mathcal{C} = \begin{pmatrix} 0 & -\mathcal{C}_{\mathbf{E}} \\ \mathcal{C}_{\mathbf{H}} & 0 \end{pmatrix} = \begin{pmatrix} 0 & -\mu^{-1}\operatorname{curl} \\ \varepsilon^{-1}\operatorname{curl} & 0 \end{pmatrix}, \tag{3.3a}$$

and endowed with the domain

$$D(\mathcal{C}) = D(\mathcal{C}_{\mathbf{H}}) \times D(\mathcal{C}_{\mathbf{E}}) = H(\operatorname{curl}, \Omega) \times H_0(\operatorname{curl}, \Omega). \tag{3.3b}$$

In both (2.1) and (3.2) we omitted the so-called divergence conditions and the boundary condition for $\mathbf{H}$ since they can be neglected in examining the time evolution of Maxwell's equations. In fact, they only have to ensured for the initial values $\mathbf{H}^0$, $\mathbf{E}^0$; cf. [25].

We make the following assumptions on the data: For the initial value and the current density we assume

$$\mathbf{u}^0 \in D(\mathcal{C}), \qquad \mathbf{J} \in C^1(0, T; L^2(\Omega)^3) \text{ or } \mathbf{J} \in C(0, T; D(\mathcal{C}_{\mathbf{E}})), \tag{3.4}$$

respectively, and for the material coefficients we demand

$$\mu, \varepsilon \in L^\infty(\Omega), \qquad \mu, \varepsilon \geq \delta > 0, \tag{3.5}$$

for a constant $\delta > 0$. These assumptions guarantee that there exists a unique solution $\mathbf{u} = (\mathbf{H}, \mathbf{E}) \in C^1(0, T; L^2(\Omega)^6) \cap C(0, T; D(\mathcal{C}))$ of (3.2) [29, Corollaries 2.5, 2.6] which is bounded by

$$\|\mathbf{u}(t)\|_{\mu\times\varepsilon}^2 \leq \mathrm{e}^1 \left(\|\mathbf{u}^0\|_{\mu\times\varepsilon}^2 + \frac{T+1}{\delta} \int_0^t \|\mathbf{J}(s)\|^2 \, ds \right). \tag{3.6}$$

It is well known that the Maxwell operator $\mathcal{C}$ is skew-adjoint w.r.t. $\big(\cdot,\cdot\big)_{\mu\times\varepsilon}$, which can be expressed in terms of the curl-operators $\mathcal{C}_{\mathbf{H}}$, $\mathcal{C}_{\mathbf{E}}$ as

$$\big(\mathcal{C}_{\mathbf{H}}\mathbf{H}, \mathbf{E}\big)_{\varepsilon} = \big(\mathbf{H}, \mathcal{C}_{\mathbf{E}}\mathbf{E}\big)_{\mu}, \qquad \mathbf{H} \in D(\mathcal{C}_{\mathbf{H}}),\ \mathbf{E} \in D(\mathcal{C}_{\mathbf{E}}). \tag{3.7}$$

4. Spatial discretization

In this section we discretize (2.1) in space with a dG method; see the textbooks [8, 20]. As a first step, we give the discrete setting in which the dG discretization can be formulated.

4.1. **Discrete setting.** We assume that Ω is approximated by a polyhedron in $\mathbb{R}^d$ which we denote by Ω again, for simplicity. We equip Ω with a simplicial mesh $\mathcal{T}_h = \{K\}$ consisting of elements K. We point out that the restriction to simplicial meshes can be dropped and all following results hold true for more general meshes satisfying the shape and contact regularity assumptions from [8, Section 1.4.1]. We denote with h_K the diameter of a mesh element K and refer to the maximal diameter by $h = \max_{K\in\mathcal{T}_h} h_K$. Moreover, we collect the faces of the mesh elements in $\mathcal{F}_h = \mathcal{F}_h^{\mathrm{int}} \cup \mathcal{F}_h^{\mathrm{bnd}}$, where the first set collects the interior faces and the second set the boundary faces. By

$$N_\partial = \max_{K\in\mathcal{T}_h} \operatorname{card}\{F \in \mathcal{F}_h \mid F \subset \partial K\}$$

we denote the maximum number of mesh faces composing the boundary of a mesh element. For simplicial meshes N_∂ is a constant. For every interior face $F \in \mathcal{F}_h^{\text{int}}$ we choose arbitrarily one of the outer unit normals of the two mesh elements composing the face F. We fix this normal and denote it with n_F. For the remaining paper we will refer to the two neighboring elements sharing the face F by K and K_F whereby the unit normal n_F points from K to K_F. For a boundary face the orientation of n_F is always outwards.

We use the discrete approximation space

$$V_h = \left\{ v_h \in L^2(\Omega) \mid v_h|_K \in \mathbb{P}_k(K) \text{ for all } K \in \mathcal{T}_h \right\}^3, \tag{4.1}$$

where $\mathbb{P}_k$ denotes the set of polynomials of degree at most k. Because we have $V_h^2 \not\subset D(\mathcal{C})$ our space discretization is nonconforming. Similarly, we write

$$H^q(\mathcal{T}_h) = \left\{ v \in L^2(\Omega) \mid v|_K \in H^q(K) \text{ for all } K \in \mathcal{T}_h \right\}, \qquad q \in \mathbb{N}, \tag{4.2}$$

for the broken Sobolev spaces fitting to the mesh $\mathcal{T}_h$. These spaces are Hilbert spaces when endowed with the norm

$$\|v\|_q^2 = \sum_{j=0}^{q} |v|_j^2, \qquad |v|_q^2 = \sum_{K \in \mathcal{T}_h} |v|_{q,K}^2 = \sum_{K \in \mathcal{T}_h} |v|_{H^q(K)}^2. \tag{4.3}$$

Furthermore, we define the spaces

$$V_\star^{\mathbf{H}} = D(\mathcal{C}_{\mathbf{H}}) \cap H^1(\mathcal{T}_h)^3, \quad V_\star^{\mathbf{E}} = D(\mathcal{C}_{\mathbf{E}}) \cap H^1(\mathcal{T}_h)^3, \quad V_\star = V_\star^{\mathbf{H}} \times V_\star^{\mathbf{E}}, \tag{4.4a}$$

and

$$V_{\star,h}^{\mathbf{H}} = V_\star^{\mathbf{H}} + V_h, \qquad V_{\star,h}^{\mathbf{E}} = V_\star^{\mathbf{E}} + V_h, \qquad V_{\star,h} = V_{\star,h}^{\mathbf{H}} \times V_{\star,h}^{\mathbf{E}}. \tag{4.4b}$$

Remark 4.1. It is also possible to vary the polynomial degree between the elements. For instance, if the solution lacks regularity in parts of the domain, one could use small polynomial degrees there. The larger errors can be compensated by using smaller mesh elements; cf. [28] for the wave equation.

For the sake of presentation, we restrict ourselves to using the same degree k in each element and assume that the solution is in $H^{k+1}(\mathcal{T}_h)$. However, since our bounds are given elementwise, it is easy to generalize our analysis to varying polynomial degrees.

Assumption 4.2. We suppose that the coefficients μ and ε are piecewise constant and that the mesh $\mathcal{T}_h$ is matched to them such that $\mu|_K \equiv \mu_K$ and $\varepsilon|_K \equiv \varepsilon_K$ are constant for each $K \in \mathcal{T}_h$.

The L^2-orthogonal projection $\pi_h : L^2(\Omega)^3 \to V_h$ onto V_h is defined such that for $\mathbf{V} \in L^2(\Omega)^3$,

$$\big(\mathbf{V} - \pi_h \mathbf{V}, \varphi_h\big) = 0 \qquad \text{for all} \quad \varphi_h \in V_h. \tag{4.5}$$

For piecewise constant coefficients we then have

$$\big(\mathbf{V} - \pi_h \mathbf{V}, \varphi_h\big)_\mu = \big(\mathbf{V} - \pi_h \mathbf{V}, \varphi_h\big)_\varepsilon = 0 \qquad \text{for all} \quad \varphi_h \in V_h. \tag{4.6}$$

For the data in (2.3) we use the L^2-projection of the continuous initial value and of the source term, i.e., $\mathbf{H}_h^0 = \pi_h \mathbf{H}^0$, $\mathbf{E}_h^0 = \pi_h \mathbf{E}^0$ and $\mathbf{J}_h = \pi_h(\varepsilon^{-1}\mathbf{J})$.

Given a piecewise constant weight function ω, $\omega|_K \equiv \omega_K$ for all $K \in \mathcal{T}_h$, we define the weighted average of a function v over an interior face $F \in \mathcal{F}_h^{\mathrm{int}}$ as

$$\{\!\{v\}\!\}_F^{\omega} = \frac{\omega_K (v|_K)|_F + \omega_{K_F}(v|_{K_F})|_F}{\omega_K + \omega_{K_F}},$$

and the jump of v over F as

$$[\![v]\!]_F = (v|_{K_F})|_F - (v|_K)|_F.$$

For vector fields these operations act componentwise.

4.2. **Discrete curl and stabilization operators.** We follow [19, 23] for the succeeding definitions. Let

$$a_F = \frac{1}{\varepsilon_K c_K + \varepsilon_{K_F} c_{K_F}}, \quad b_F = \frac{1}{\mu_K c_K + \mu_{K_F} c_{K_F}} \quad \text{for all} \quad F \in \mathcal{F}_h^{\mathrm{int}}, \tag{4.7a}$$

$$b_F = \frac{1}{\mu_K c_K} \quad \text{for all} \quad F \in \mathcal{F}_h^{\mathrm{bnd}}. \tag{4.7b}$$

For $(\mathbf{H}_h, \mathbf{E}_h) \in V_h^2$ and $(\phi_h, \psi_h) \in V_h^2$ we define the discrete curl-operators $\boldsymbol{\mathcal{C}}_{\mathbf{H}}, \boldsymbol{\mathcal{C}}_{\mathbf{E}} : V_h \to V_h$ as

$$\big(\boldsymbol{\mathcal{C}}_{\mathbf{H}} \mathbf{H}_h, \psi_h\big)_{\varepsilon} = \sum_{K \in \mathcal{T}_h} \big(\operatorname{curl} \mathbf{H}_h, \psi_h\big)_K + \sum_{F \in \mathcal{F}_h^{\mathrm{int}}} \big(n_F \times [\![\mathbf{H}_h]\!]_F, \{\!\{\psi_h\}\!\}_F^{\varepsilon c}\big)_F \tag{4.8a}$$

and

$$\begin{aligned}\big(\boldsymbol{\mathcal{C}}_{\mathbf{E}} \mathbf{E}_h, \phi_h\big)_{\mu} = &\sum_{K \in \mathcal{T}_h} \big(\operatorname{curl} \mathbf{E}_h, \phi_h\big)_K \\ &+ \sum_{F \in \mathcal{F}_h^{\mathrm{int}}} \big(n_F \times [\![\mathbf{E}_h]\!]_F, \{\!\{\phi_h\}\!\}_F^{\mu c}\big)_F - \sum_{F \in \mathcal{F}_h^{\mathrm{bnd}}} \big(n_F \times \mathbf{E}_h, \phi_h\big)_F .\end{aligned} \tag{4.8b}$$

Moreover, we introduce the stabilization operators $\boldsymbol{\mathcal{S}}_{\mathbf{H}}, \boldsymbol{\mathcal{S}}_{\mathbf{E}} : V_h \to V_h$ by

$$\big(\boldsymbol{\mathcal{S}}_{\mathbf{H}} \mathbf{H}_h, \phi_h\big)_{\mu} = \sum_{F \in \mathcal{F}_h^{\mathrm{int}}} a_F \big(n_F \times [\![\mathbf{H}_h]\!]_F, n_F \times [\![\phi_h]\!]_F\big)_F \tag{4.9a}$$

and

$$\begin{aligned}\big(\boldsymbol{\mathcal{S}}_{\mathbf{E}} \mathbf{E}_h, \psi_h\big)_{\varepsilon} = &\sum_{F \in \mathcal{F}_h^{\mathrm{int}}} b_F \big(n_F \times [\![\mathbf{E}_h]\!]_F, n_F \times [\![\psi_h]\!]_F\big)_F \\ &+ \sum_{F \in \mathcal{F}_h^{\mathrm{bnd}}} b_F \big(n_F \times \mathbf{E}_h, n_F \times \psi_h\big)_F .\end{aligned} \tag{4.9b}$$

We collect the above introduced operators in

$$\boldsymbol{\mathcal{C}} = \begin{pmatrix} \mathbf{0} & -\boldsymbol{\mathcal{C}}_{\mathbf{E}} \\ \boldsymbol{\mathcal{C}}_{\mathbf{H}} & \mathbf{0} \end{pmatrix}, \qquad \boldsymbol{\mathcal{S}} = \begin{pmatrix} \boldsymbol{\mathcal{S}}_{\mathbf{H}} & \mathbf{0} \\ \mathbf{0} & \boldsymbol{\mathcal{S}}_{\mathbf{E}} \end{pmatrix}.$$

The operators given in (4.8), (4.9) are also well-defined on $V_\star^{\mathbf{H}}$ and $V_\star^{\mathbf{E}}$, respectively, i.e., $\boldsymbol{\mathcal{C}}_{\mathbf{H}}, \boldsymbol{\mathcal{S}}_{\mathbf{H}} : V_\star^{\mathbf{H}} \to V_h$, $\boldsymbol{\mathcal{C}}_{\mathbf{E}}, \boldsymbol{\mathcal{S}}_{\mathbf{E}} : V_\star^{\mathbf{E}} \to V_h$. Since functions in these spaces have vanishing tangential jumps,

$$n_F \times [\![\mathbf{H}]\!]_F = n_F \times [\![\mathbf{E}]\!]_F = 0, \qquad \mathbf{H} \in V_\star^{\mathbf{H}},\ \mathbf{E} \in V_\star^{\mathbf{E}}, \tag{4.10}$$

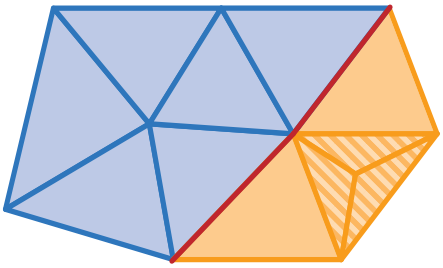

FIGURE 1. Decomposition of the mesh elements. The striped elements indicate the fine elements collected in $\mathcal{T}_{h,f}$, whereas the non-striped ones mark the coarse elements of $\mathcal{T}_{h,c}$. In blue we illustrate the explicitly treated elements of $\mathcal{T}_{h,e}$ and in orange the implicitly treated elements of $\mathcal{T}_{h,i}$ and the same color code is used for the faces $\mathcal{F}_{h,e}^{\mathrm{int}}$ and $\mathcal{F}_{h,i}^{\mathrm{int}}$, respectively. The coarse elements of $\mathcal{T}_{h,ci}$ which are treated implicitly are marked in dark orange, non-striped and the faces of $\mathcal{F}_{h,ci}^{\mathrm{int}}$ are red.

the following consistency properties hold true:

(4.11)
$$\boldsymbol{\mathcal{C}}_{\mathbf{H}}\mathbf{H} = \pi_h \mathcal{C}_{\mathbf{H}}\mathbf{H}, \quad \boldsymbol{\mathcal{C}}_{\mathbf{E}}\mathbf{E} = \pi_h \mathcal{C}_{\mathbf{E}}\mathbf{E}, \quad \boldsymbol{\mathcal{S}}_{\mathbf{H}}\mathbf{H} = \boldsymbol{\mathcal{S}}_{\mathbf{E}}\mathbf{E} = 0, \quad \mathbf{H} \in V_\star^{\mathbf{H}},\ \mathbf{E} \in V_\star^{\mathbf{E}}.$$

The next lemma gives a partial integration formula for the discrete curl-operators $\boldsymbol{\mathcal{C}}_{\mathbf{H}}$ and $\boldsymbol{\mathcal{C}}_{\mathbf{E}}$.

Lemma 4.3. *Let* $(\mathbf{H}, \mathbf{E}) \in V_{\star,h}^{\mathbf{H}} \times V_{\star,h}^{\mathbf{E}}$ *and* $(\phi_h, \psi_h) \in V_h^2$. *Then, we have that*

$$\begin{aligned}\big(\boldsymbol{\mathcal{C}}_{\mathbf{H}}\mathbf{H}, \psi_h\big)_\varepsilon &= \sum_{K\in\mathcal{T}_h} \big(\operatorname{curl}\psi_h, \mathbf{H}\big)_K \\ &\quad + \sum_{F\in\mathcal{F}_h^{\mathrm{int}}} \big(n_F \times [\![\psi_h]\!]_F, \{\!\{\mathbf{H}\}\!\}_F^{\mu c}\big)_F - \sum_{F\in\mathcal{F}_h^{\mathrm{bnd}}} \big(n_F\times\psi_h, \mathbf{H}\big)_F\end{aligned} \tag{4.12a}$$

and

$$\big(\boldsymbol{\mathcal{C}}_{\mathbf{E}}\mathbf{E}, \phi_h\big)_\mu = \sum_{K\in\mathcal{T}_h} \big(\operatorname{curl}\phi_h, \mathbf{E}\big)_K + \sum_{F\in\mathcal{F}_h^{\mathrm{int}}} \big(n_F \times [\![\phi_h]\!]_F, \{\!\{\mathbf{E}\}\!\}_F^{\varepsilon c}\big)_F\,. \tag{4.12b}$$

Proof. Partial integration (see the proof of [24, Lemma 2.2]). □

This lemma and (4.8) show that the discrete curl-operator $\boldsymbol{\mathcal{C}}$ preserves (on the space V_h^2) the skew-adjointness of the continuous Maxwell operator (3.7). In fact, for $\mathbf{u}_h = (\mathbf{H}_h, \mathbf{E}_h) \in V_h^2$ we have

$$\big(\boldsymbol{\mathcal{C}}_{\mathbf{H}}\mathbf{H}_h, \mathbf{E}_h\big)_\varepsilon = \big(\mathbf{H}_h, \boldsymbol{\mathcal{C}}_{\mathbf{E}}\mathbf{E}_h\big)_\mu, \qquad \big(\boldsymbol{\mathcal{C}}\mathbf{u}_h, \mathbf{u}_h\big)_{\mu\times\varepsilon} = 0. \tag{4.13}$$

The stabilization operators $\boldsymbol{\mathcal{S}}_{\mathbf{H}}$, $\boldsymbol{\mathcal{S}}_{\mathbf{E}}$ are symmetric and positive semidefinite on V_h, i.e., for $\mathbf{H}_h, \mathbf{E}_h, \widehat{\mathbf{H}}_h, \widehat{\mathbf{E}}_h \in V_h$ we have

$$\big(\boldsymbol{\mathcal{S}}_{\mathbf{H}}\mathbf{H}_h, \widehat{\mathbf{H}}_h\big)_\mu = \big(\mathbf{H}_h, \boldsymbol{\mathcal{S}}_{\mathbf{H}}\widehat{\mathbf{H}}_h\big)_\mu, \qquad \big(\boldsymbol{\mathcal{S}}_{\mathbf{E}}\mathbf{E}_h, \widehat{\mathbf{E}}_h\big)_\varepsilon = \big(\mathbf{E}_h, \boldsymbol{\mathcal{S}}_{\mathbf{E}}\widehat{\mathbf{E}}_h\big)_\varepsilon \tag{4.14a}$$

and

$$\big(\boldsymbol{\mathcal{S}}_{\mathbf{H}}\mathbf{H}_h, \mathbf{H}_h\big)_\mu \geq 0, \qquad \big(\boldsymbol{\mathcal{S}}_{\mathbf{E}}\mathbf{E}_h, \mathbf{E}_h\big)_\varepsilon \geq 0. \tag{4.14b}$$

4.3. **Splitting of discrete operators.** Recall that we are interested in the situation where the mesh is split into a coarse and a fine part, and where the number of fine elements is small compared to the number of coarse ones; see (2.4). As pointed out in [24] it is necessary to treat the fine elements *and* their neighbors implicitly in order to obtain a scheme with a CFL condition independent of the fine part $\mathcal{T}_{h,f}$. This leads to the decomposition of $\mathcal{T}_h = \mathcal{T}_{h,i} \,\dot\cup\, \mathcal{T}_{h,e}$, where

$$\mathcal{T}_{h,i} = \{K \in \mathcal{T}_h \mid \exists K_f \in \mathcal{T}_{h,f} \ : \ \mathrm{vol}_{d-1}(\partial K \cap \partial K_f) \neq 0\}, \qquad \mathcal{T}_{h,e} = \mathcal{T}_h \setminus \mathcal{T}_{h,i};$$

see [24, Definition 2.3]. The elements in $\mathcal{T}_{h,i}$ are treated implicitly and the ones from $\mathcal{T}_{h,e}$ can be integrated explicitly. In the following we will frequently use the set of implicitly treated elements which share a face with at least one explicitly treated element

$$\mathcal{T}_{h,ci} = \{K_i \in \mathcal{T}_{h,i} \mid \exists K_e \in \mathcal{T}_{h,e} \ : \ \mathrm{vol}_{d-1}(\partial K_e \cap \partial K_i) \neq 0\}.$$

We note the following relations between the sets of mesh elements:

$$\mathcal{T}_{h,e} \subset \mathcal{T}_{h,c}, \qquad \mathcal{T}_{h,f} \subset \mathcal{T}_{h,i}, \qquad \mathcal{T}_{h,i} \cap \mathcal{T}_{h,c} \neq \emptyset, \qquad \mathcal{T}_{h,ci} \subset \mathcal{T}_{h,c} \cap \mathcal{T}_{h,i}.$$

Analogous to [24, Definition 2.4] we decompose the interior mesh faces into

$$\mathcal{F}_h^{\mathrm{int}} = \mathcal{F}_{h,i}^{\mathrm{int}} \,\dot\cup\, \mathcal{F}_{h,e}^{\mathrm{int}} \,\dot\cup\, \mathcal{F}_{h,ci}^{\mathrm{int}}, \tag{4.15a}$$

where $\mathcal{F}_{h,i}^{\mathrm{int}}$ contains the faces between implicitly treated elements, $\mathcal{F}_{h,e}^{\mathrm{int}}$ the faces between explicitly treated elements and $\mathcal{F}_{h,ci}^{\mathrm{int}}$ the faces bordering an explicitly and an implicitly treated element. We use the convention that for a face $F \in \mathcal{F}_{h,ci}^{\mathrm{int}}$ the normal n_F is directed from the implicit element K_i towards the explicit element K_e. Similarly to the decomposition of $\mathcal{F}_h^{\mathrm{int}}$ the set $\mathcal{F}_h^{\mathrm{bnd}}$ is partitioned into

$$\mathcal{F}_h^{\mathrm{bnd}} = \mathcal{F}_{h,i}^{\mathrm{bnd}} \,\dot\cup\, \mathcal{F}_{h,e}^{\mathrm{bnd}}, \tag{4.15b}$$

so that $\mathcal{F}_{h,i}^{\mathrm{bnd}}$ contains the boundary faces of implicitly integrated elements and $\mathcal{F}_{h,e}^{\mathrm{bnd}}$ the boundary faces of explicitly treated elements. Moreover, we set

$$\mathcal{F}_{h,c}^{\mathrm{int}} = \mathcal{F}_{h,e}^{\mathrm{int}} \,\dot\cup\, \mathcal{F}_{h,ci}^{\mathrm{int}}, \tag{4.15c}$$

Observe that the set $\mathcal{F}_{h,c}^{\mathrm{int}}$ only contains faces bordering two coarse elements. In Figure 1 we illustrate these sets in a small example.

We denote by χ_i and χ_e the indicator functions on $\mathcal{T}_{h,i}$ and $\mathcal{T}_{h,e}$, respectively. As proposed in [24, Definition 2.6] we use these indicator functions to define split versions of the discrete curl-operators $\boldsymbol{\mathcal{C}}_{\mathbf{H}}^e, \boldsymbol{\mathcal{C}}_{\mathbf{H}}^i : V_{\star,h}^{\mathbf{H}} \to V_h$ and $\boldsymbol{\mathcal{C}}_{\mathbf{E}}^e, \boldsymbol{\mathcal{C}}_{\mathbf{E}}^i : V_{\star,h}^{\mathbf{E}} \to V_h$ by

$$\boldsymbol{\mathcal{C}}_{\mathbf{H}}^b = \boldsymbol{\mathcal{C}}_{\mathbf{H}} \circ \chi_b, \qquad \boldsymbol{\mathcal{C}}_{\mathbf{E}}^b = \chi_b \circ \boldsymbol{\mathcal{C}}_{\mathbf{E}}, \qquad b \in \{i, e\}. \tag{4.16}$$

For the definition of the split discrete curl-operators the usage of the indicator functions is a convenient choice. However, it is not appropriate to split the stabilization operators. From (4.9) we observe that the stabilization operators solely take values of the functions on faces into account. Hence, it is natural to construct explicit stabilization operators by replacing the sums over all faces by sums over faces belonging to explicitly treated elements, i.e., by the sets $\mathcal{F}_{h,c}^{\mathrm{int}}$ and $\mathcal{F}_{h,e}^{\mathrm{bnd}}$. This motivates the following definition.

Definition 4.4. We define the explicit stabilization operators $\boldsymbol{\mathcal{S}}^e_{\mathbf{H}} : V^{\mathbf{H}}_{\star,h} \to V_h$ such that for all $\phi_h \in V_h$,

$$\big(\boldsymbol{\mathcal{S}}^e_{\mathbf{H}}\mathbf{H}, \phi_h\big)_\mu = \sum_{F\in\mathcal{F}^{\mathrm{int}}_{h,c}} a_F\big(n_F \times [\![\mathbf{H}]\!]_F, n_F \times [\![\phi_h]\!]_F\big)_F \,, \tag{4.17a}$$

and $\boldsymbol{\mathcal{S}}^e_{\mathbf{E}} : V^{\mathbf{E}}_{\star,h} \to V_h$ such that for all $\psi_h \in V_h$,

$$\begin{aligned}\big(\boldsymbol{\mathcal{S}}^e_{\mathbf{E}}\mathbf{E}, \psi_h\big)_\varepsilon = &\sum_{F\in\mathcal{F}^{\mathrm{int}}_{h,c}} b_F\big(n_F \times [\![\mathbf{E}]\!]_F, n_F \times [\![\psi_h]\!]_F\big)_F \\ &+ \sum_{F\in\mathcal{F}^{\mathrm{bnd}}_{h,e}} b_F\big(n_F \times \mathbf{E}, n_F \times \psi_h\big)_F \,,\end{aligned} \tag{4.17b}$$

where a_F and b_F were defined in (4.7). Moreover, we define

$$\boldsymbol{\mathcal{S}}^e : V_{\star,h} \to V_h^2, \qquad \boldsymbol{\mathcal{S}}^e = \begin{pmatrix} \boldsymbol{\mathcal{S}}^e_{\mathbf{H}} & 0 \\ 0 & \boldsymbol{\mathcal{S}}^e_{\mathbf{E}} \end{pmatrix}. \tag{4.17c}$$

Let us give some properties of the above introduced operators: For the split curl-operators we have that

$$\boldsymbol{\mathcal{C}}_{\mathbf{H}} = \boldsymbol{\mathcal{C}}^i_{\mathbf{H}} + \boldsymbol{\mathcal{C}}^e_{\mathbf{H}}, \qquad \boldsymbol{\mathcal{C}}_{\mathbf{E}} = \boldsymbol{\mathcal{C}}^i_{\mathbf{E}} + \boldsymbol{\mathcal{C}}^e_{\mathbf{E}}, \qquad \boldsymbol{\mathcal{C}}^b_{\mathbf{H}}\boldsymbol{\mathcal{C}}_{\mathbf{E}} = \boldsymbol{\mathcal{C}}^b_{\mathbf{H}}\boldsymbol{\mathcal{C}}^b_{\mathbf{E}}, \quad b \in \{e, i\}. \tag{4.18}$$

Furthermore, observe that by (4.10) the operators $\boldsymbol{\mathcal{C}}^e_{\mathbf{E}}$, $\boldsymbol{\mathcal{C}}^i_{\mathbf{E}}$ and $\boldsymbol{\mathcal{S}}^e_{\mathbf{H}}$, $\boldsymbol{\mathcal{S}}^e_{\mathbf{E}}$ preserve the consistency of the full operators (4.11). In particular, for the stabilization operators we have

$$\boldsymbol{\mathcal{S}}^e_{\mathbf{H}}\mathbf{H} = \boldsymbol{\mathcal{S}}^e_{\mathbf{E}}\mathbf{E} = 0, \qquad \mathbf{H} \in V^{\mathbf{H}}_\star, \quad \mathbf{E} \in V^{\mathbf{E}}_\star. \tag{4.19}$$

Last, all operators preseve the adjointness and the symmetry properties on V_h of the full operators (4.13) and (4.14a), respectively, i.e., for $\mathbf{H}_h, \mathbf{E}_h, \widehat{\mathbf{H}}_h, \widehat{\mathbf{E}}_h \in V_h$ we have

$$\big(\boldsymbol{\mathcal{C}}^e_{\mathbf{H}}\mathbf{H}_h, \mathbf{E}_h\big)_\varepsilon = \big(\mathbf{H}_h, \boldsymbol{\mathcal{C}}^e_{\mathbf{E}}\mathbf{E}_h\big)_\mu, \qquad \big(\boldsymbol{\mathcal{C}}^i_{\mathbf{H}}\mathbf{H}_h, \mathbf{E}_h\big)_\varepsilon = \big(\mathbf{H}_h, \boldsymbol{\mathcal{C}}^i_{\mathbf{E}}\mathbf{E}_h\big)_\mu, \tag{4.20a}$$

$$\big(\boldsymbol{\mathcal{S}}^e_{\mathbf{H}}\mathbf{H}_h, \widehat{\mathbf{H}}_h\big)_\mu = \big(\mathbf{H}_h, \boldsymbol{\mathcal{S}}^e_{\mathbf{H}}\widehat{\mathbf{H}}_h\big)_\mu, \qquad \big(\boldsymbol{\mathcal{S}}^e_{\mathbf{E}}\mathbf{E}_h, \widehat{\mathbf{E}}_h\big)_\varepsilon = \big(\mathbf{E}_h, \boldsymbol{\mathcal{S}}^e_{\mathbf{E}}\widehat{\mathbf{E}}_h\big)_\varepsilon. \tag{4.20b}$$

Moreover, $\boldsymbol{\mathcal{S}}^e_{\mathbf{H}}$ and $\boldsymbol{\mathcal{S}}^e_{\mathbf{E}}$ also inherit the positive semidefiniteness of $\boldsymbol{\mathcal{S}}_{\mathbf{H}}$ and $\boldsymbol{\mathcal{S}}_{\mathbf{E}}$, respectively. This motivates to introduce seminorms associated with the explicit stabilization operators.

Definition 4.5. For $\mathbf{u} = (\mathbf{H}, \mathbf{E}) \in V_{\star,h}$ we define the seminorms

$$|\mathbf{H}|^2_{\boldsymbol{\mathcal{S}}^e_{\mathbf{H}}} = \sum_{F\in\mathcal{F}^{\mathrm{int}}_{h,c}} a_F \|n_F \times [\![\mathbf{H}]\!]_F\|^2_F \,, \tag{4.21a}$$

$$|\mathbf{E}|^2_{\boldsymbol{\mathcal{S}}^e_{\mathbf{E}}} = \sum_{F\in\mathcal{F}^{\mathrm{int}}_{h,c}} b_F \|n_F \times [\![\mathbf{E}]\!]_F\|^2_F + \sum_{F\in\mathcal{F}^{\mathrm{bnd}}_{h,e}} b_F \|n_F \times \mathbf{E}\|^2_F \,. \tag{4.21b}$$

Moreover, we set

$$|\mathbf{u}|^2_{\boldsymbol{\mathcal{S}}^e} = |\mathbf{H}|^2_{\boldsymbol{\mathcal{S}}^e_{\mathbf{H}}} + |\mathbf{E}|^2_{\boldsymbol{\mathcal{S}}^e_{\mathbf{E}}} \,. \tag{4.21c}$$

For $\mathbf{u}_h = (\mathbf{H}_h, \mathbf{E}_h) \in V_h^2$ we have that

$$\begin{aligned} |\mathbf{H}_h|^2_{\boldsymbol{\mathcal{S}}^e_{\mathbf{H}}} &= \big(\boldsymbol{\mathcal{S}}^e_{\mathbf{H}}\mathbf{H}_h, \mathbf{H}_h\big)_\mu \,, \qquad |\mathbf{E}_h|^2_{\boldsymbol{\mathcal{S}}^e_{\mathbf{E}}} = \big(\boldsymbol{\mathcal{S}}^e_{\mathbf{E}}\mathbf{E}_h, \mathbf{E}_h\big)_\varepsilon \,, \\ |\mathbf{u}_h|^2_{\boldsymbol{\mathcal{S}}^e} &= \big(\boldsymbol{\mathcal{S}}^e\mathbf{u}_h, \mathbf{u}_h\big)_{\mu\times\varepsilon} \,. \end{aligned} \tag{4.22}$$

4.4. **Bounds on discrete operators.** We end this section by providing bounds on the explicit split discrete curl-operators and on the explicit stabilization operators. Both operators act on the mesh elements and on the mesh faces of the spatial grid, so these bounds will require a certain quality of our spatial mesh [8, Definition 1.38].

Assumption 4.6. We assume that the mesh $\mathcal{T}_h$ is shape regular, which means that there exist constants $\rho, \rho_c > 0$ independent of h such that

$$\frac{h_K}{r_K} \le \rho, \quad K \in \mathcal{T}_h, \qquad\qquad \frac{h_K}{r_K} \le \rho_c, \quad K \in \mathcal{T}_{h,c},$$

where r_K denotes the radius of the largest ball inscribed in K.

We have $\rho \ge \rho_c$ and for locally refined meshes we might have $\rho \gg \rho_c$. By Assumption 4.6 we can bound the average of the diameters of the neighboring elements by the maximum and the minimum diameter of the elements,

$$\rho^{-1} \max(h_K, h_{K_F}) \le \frac{h_K + h_{K_F}}{2} \le \rho \min(h_K, h_{K_F}), \qquad K, K_F \in \mathcal{T}_h. \tag{4.23}$$

On the coarse grid $\mathcal{T}_{h,c}$ this inequality holds true with ρ_c instead of ρ. Two crucial inequalities for functions in V_h are the inverse inequality

$$\|\operatorname{curl} \mathbf{U}_h\|_K \le C_{\mathrm{inv}} h_K^{-1} \|\mathbf{U}_h\|_K, \qquad K \in \mathcal{T}_h,\ \mathbf{U}_h \in V_h, \tag{4.24}$$

and the discrete trace inequality

$$\|\mathbf{U}_h\|_F \le C_{\mathrm{tr}} h_K^{-1/2} \|\mathbf{U}_h\|_K, \qquad F \in \mathcal{F}_h,\ \mathbf{U}_h \in V_h; \tag{4.25}$$

see [8, Lemmas 1.44, 1.46]. The bound (4.25) also holds for K_F. The constants C_{inv} and C_{tr} depend on the mesh regularity constant ρ, the polynomial degree k and the dimension d. On the coarse mesh $\mathcal{T}_{h,c}$ these inequalities hold true with dependency on ρ_c, k and d. We denote the corresponding constants by $C_{\mathrm{inv},c}$ and $C_{\mathrm{tr},c}$.

Let

$$c_{\infty,c} = \max_{K \in \mathcal{T}_{h,c}} c_K, \qquad c_\infty = \max_{K \in \mathcal{T}_h} c_K$$

be the maximum speed of light in the coarse grid and in the whole grid, respectively. For $\mathbf{u}_h = (\mathbf{H}_h, \mathbf{E}_h)$ we introduce the following ℓ^p-L^2-norms scaled with the order q of the approximation

$$\|\mathbf{H}_h\|_{\mu,\mathcal{T}_h,p,q}^p = \sum_{K \in \mathcal{T}_h} h_K^{pq} \|\mathbf{H}_h\|_{\mu,K}^p, \qquad \|\mathbf{E}_h\|_{\varepsilon,\mathcal{T}_h,p,q}^p = \sum_{K \in \mathcal{T}_h} h_K^{pq} \|\mathbf{E}_h\|_{\varepsilon,K}^p, \tag{4.26a}$$

$$\|\mathbf{u}_h\|_{\mu\times\varepsilon,\mathcal{T}_h,p,q}^p = \|\mathbf{H}_h\|_{\mu,\mathcal{T}_h,p,q}^p + \|\mathbf{E}_h\|_{\varepsilon,\mathcal{T}_h,p,q}^p. \tag{4.26b}$$

Moreover, for $v \in H^m(\mathcal{T}_h)$ we define the weighted broken ℓ^p-H^m-seminorm as

$$|v|_{m,\mathcal{T}_h,p,q}^p = \sum_{K \in \mathcal{T}_h} h_K^{pq} |v|_{m,K}^p. \tag{4.26c}$$

Note that for our $H^m(\mathcal{T}_h)$-seminorm we have $|v|_m = |v|_{m,\mathcal{T}_h,2,0}$; see (4.3). Now, we give two boundedness results, one for the L^2-norm of the explicit curl-operators $\boldsymbol{\mathcal{C}}_{\mathbf{H}}^e$ and $\boldsymbol{\mathcal{C}}_{\mathbf{E}}^e$, and one for the explicit stabilization seminorm $|\cdot|_{\boldsymbol{\mathcal{S}}^e}$. It is crucial to observe that these bounds hold true independent of the fine mesh $\mathcal{T}_{h,f}$.

Theorem 4.7. *For $\mathbf{H}_h, \mathbf{E}_h \in V_h$ we have the bounds*

$$\|\boldsymbol{\mathcal{C}}^e_{\mathbf{H}}\mathbf{H}_h\|_\varepsilon \leq C_{\mathrm{bnd},c}c_{\infty,c}\|\mathbf{H}_h\|_{\mu,\mathcal{T}_{h,c},2,-1}, \tag{4.27a}$$

$$\|\boldsymbol{\mathcal{C}}^e_{\mathbf{E}}\mathbf{E}_h\|_\mu \leq C_{\mathrm{bnd},c}c_{\infty,c}\|\mathbf{E}_h\|_{\varepsilon,\mathcal{T}_{h,c},2,-1}. \tag{4.27b}$$

Furthermore, for $\mathbf{u}_h \in V_h^2$ we have

$$|\mathbf{u}_h|_{\boldsymbol{\mathcal{S}}^e} \leq \left(\widehat{C}_{\mathrm{bnd},c}c_{\infty,c}\right)^{1/2}\|\mathbf{u}_h\|_{\mu\times\varepsilon,\mathcal{T}_{h,c},2,-\frac{1}{2}}. \tag{4.28}$$

The constants are given by $C_{\mathrm{bnd},c} = C_{\mathrm{inv},c} + 2C^2_{\mathrm{tr},c}N_\partial\rho_c$ and $\widehat{C}_{\mathrm{bnd},c} = 2C^2_{\mathrm{tr},c}N_\partial$.

Proof. The bounds (4.27) are shown in [24, Theorem 2.7] and (4.28) is proven in Appendix B. □

Last, we provide a bound on terms involving an inner product of a projection error $\mathbf{e}_\pi = \mathbf{u} - \pi_h\mathbf{u}$, $\mathbf{u} \in V_\star$, with a dG function $\varphi_h \in V_h^2$.

Theorem 4.8. *Let $\mathbf{u} \in V_\star \cap H^{k+1}(\mathcal{T}_h)^6$. Then, for all $\varphi_h \in V_h^2$ we have*

$$\begin{aligned}\left(\boldsymbol{\mathcal{C}}\mathbf{e}_\pi, \varphi_h\right)_{\mu\times\varepsilon} \leq& C_{\pi,c}|\varphi_h|_{\boldsymbol{\mathcal{S}}^e}|\mathbf{u}|_{k+1,\mathcal{T}_{h,e}\cup\mathcal{T}_{h,ci},2,k+\frac{1}{2}}\\ &+ \widehat{C}_\pi\|\varphi_h\|_{\mu\times\varepsilon,\mathcal{T}_{h,i}}|\mathbf{u}|_{k+1,\mathcal{T}_{h,i},2,k}\end{aligned} \tag{4.29}$$

and

$$\left(\boldsymbol{\mathcal{S}}^e\mathbf{e}_\pi, \varphi_h\right)_{\mu\times\varepsilon} \leq C_{\pi,c}|\varphi_h|_{\boldsymbol{\mathcal{S}}^e}|u|_{k+1,\mathcal{T}_{h,e}\cup\mathcal{T}_{h,ci},2,k+\frac{1}{2}}. \tag{4.30}$$

The constants are given by $C_{\pi,c} = \left(2N_\partial c_{\infty,c}\right)^{1/2}\widehat{C}_{\mathrm{app}}$ and $\widehat{C}_\pi = 2\widehat{C}_{\mathrm{app}}C_{\mathrm{tr}}N_\partial c_\infty\rho$.

Remark 4.9. The bound (4.29) yields only the convergence rate k on the (few) coarse elements in $\mathcal{T}_{h,ci}$. It also might happen that a small amount of coarse mesh elements belongs to $\mathcal{T}_{h,i} \setminus \mathcal{T}_{h,ci}$ (e.g., if a coarse mesh element possesses only fine neighbors). However, an advantage of dG methods is their flexibility in choosing a different polynomial degree on each mesh element. As a consequence, if we choose the polynomial degree $k+1$ on the (small number of) mesh elements in $\mathcal{T}_{h,c} \cap \mathcal{T}_{h,i}$, we obtain the rate $k+1/2$ on the whole coarse set. Particularly, we obtain

$$\begin{aligned}\left(\boldsymbol{\mathcal{C}}\mathbf{e}_\pi, \varphi_h\right)_{\mu\times\varepsilon} \leq& C_{\pi,c}|\varphi_h|_{\boldsymbol{\mathcal{S}}^e}|\mathbf{u}|_{k+1,\mathcal{T}_{h,c},2,k+\frac{1}{2}}\\ &+ \widehat{C}_\pi\|\varphi_h\|_{\mu\times\varepsilon,\mathcal{T}_{h,i}}|\mathbf{u}|_{k+1,\mathcal{T}_{h,f},2,k}\end{aligned} \tag{4.31}$$

and

$$\left(\boldsymbol{\mathcal{S}}^e\mathbf{e}_\pi, \varphi_h\right)_{\mu\times\varepsilon} \leq C_{\pi,c}|\varphi_h|_{\boldsymbol{\mathcal{S}}^e}|u|_{k+1,\mathcal{T}_{h,c},2,k+\frac{1}{2}}. \tag{4.32}$$

In the following we will use (for a shorter notation) the bounds (4.29) and (4.30) w.r.t. the set $\mathcal{T}_{h,c}$ instead of $\mathcal{T}_{h,e} \cup \mathcal{T}_{h,ci}$, and leave it to the reader to recall that by the above idea they can be sharpened to (4.31) and (4.32), respectively.

Proof. See Appendix B. □

5. Full discretization

In the last section we established the space discretization of Maxwell's equations (2.1). So it remains to discuss the time integration. We base our time integrator on a subdivision of the time interval $[0, T]$ into equidistant intervals $[t_n, t_{n+1}]$ of length τ, where $t_n = n\tau$. We refer to τ as the time step. Now, we have all ingredients such that the fully discrete scheme (2.5) is well defined. The aim of this section is to give a stability and convergence analysis for this scheme. We point out that by

choosing $\mathcal{T}_{h,e} = \mathcal{T}_h$ the locally implicit scheme (2.5) turns to a fully stabilized, fully explicit Verlet-type method. Related ideas for the Verlet method on a staggered time grid have been presented in [2, 26]. However, the stability and convergence analysis are—to the best of our knowledge—new.

5.1. **Stability and energy dissipation.** Our first step in the analysis of the upwind fluxes locally implicit scheme (2.5) consists in casting it into a more compact form.

Lemma 5.1. *The numerical scheme* (2.5) *can be written as*

$$\boldsymbol{\mathcal{R}}_L \mathbf{u}_h^{n+1} = \boldsymbol{\mathcal{R}}_R \mathbf{u}_h^n - \tau\alpha \boldsymbol{\mathcal{S}}^e \mathbf{u}_h^n + \frac{\tau}{2}\big(\mathbf{j}_h^{n+1} + \mathbf{j}_h^n\big), \tag{5.1a}$$

where $\mathbf{j}_h^n = (0, \mathbf{J}_h^n) = (0, \mathbf{J}_h(t_n))$ *and where the operators* $\boldsymbol{\mathcal{R}}_L$, $\boldsymbol{\mathcal{R}}_R$ *are defined as*

$$\boldsymbol{\mathcal{R}}_L = \boldsymbol{\mathcal{I}} - \frac{\tau}{2}\boldsymbol{\mathcal{C}} - \frac{\tau^2}{4}\boldsymbol{\mathcal{D}}^e, \quad \boldsymbol{\mathcal{R}}_R = \boldsymbol{\mathcal{I}} + \frac{\tau}{2}\boldsymbol{\mathcal{C}} - \frac{\tau^2}{4}\boldsymbol{\mathcal{D}}^e, \tag{5.1b}$$

$$\boldsymbol{\mathcal{D}}^e = \begin{pmatrix} 0 & 0 \\ 0 & \boldsymbol{\mathcal{C}}_{\mathbf{H}}^e \boldsymbol{\mathcal{C}}_{\mathbf{E}} \end{pmatrix}.$$

Proof. Adding (2.5a) and (2.5c) yields

$$\mathbf{H}_h^{n+1} - \mathbf{H}_h^n = -\frac{\tau}{2}\boldsymbol{\mathcal{C}}_{\mathbf{E}}\big(\mathbf{E}_h^{n+1} + \mathbf{E}_h^n\big) - \tau\alpha \boldsymbol{\mathcal{S}}_{\mathbf{H}}^e \mathbf{H}_h^n,$$

which is the first component of (5.1a). For the second component we subtract (2.5c) from (2.5a):

$$\mathbf{H}_h^{n+1/2} = \frac{1}{2}\big(\mathbf{H}_h^{n+1} + \mathbf{H}_h^n\big) + \frac{\tau}{4}\boldsymbol{\mathcal{C}}_{\mathbf{E}}\big(\mathbf{E}_h^{n+1} - \mathbf{E}_h^n\big).$$

Inserting this into (2.5b) we infer

$$\mathbf{E}_h^{n+1} - \mathbf{E}_h^n = \frac{\tau}{2}\boldsymbol{\mathcal{C}}_{\mathbf{H}}(\mathbf{H}_h^{n+1} + \mathbf{H}_h^n) + \frac{\tau^2}{4}\boldsymbol{\mathcal{C}}_{\mathbf{H}}^e \boldsymbol{\mathcal{C}}_{\mathbf{E}}(\mathbf{E}_h^{n+1} - \mathbf{E}_h^n) - \tau\alpha \boldsymbol{\mathcal{S}}_{\mathbf{E}}^e \mathbf{E}_h^n - \frac{\tau}{2}(\mathbf{J}_h^{n+1} + \mathbf{J}_h^n),$$

by using $\boldsymbol{\mathcal{C}}_{\mathbf{H}}^e + \boldsymbol{\mathcal{C}}_{\mathbf{H}}^i = \boldsymbol{\mathcal{C}}_{\mathbf{H}}$; see (4.18). □

In [24, Lemma 3.2] we already elaborated the following properties of the operators $\boldsymbol{\mathcal{R}}_L$ and $\boldsymbol{\mathcal{R}}_R$:

$$\big(\boldsymbol{\mathcal{R}}_L \mathbf{u}_h, \widehat{\mathbf{u}}_h\big)_{\mu\times\varepsilon} = \big(\mathbf{u}_h, \boldsymbol{\mathcal{R}}_R \widehat{\mathbf{u}}_h\big)_{\mu\times\varepsilon} \qquad \text{for } \mathbf{u}_h, \widehat{\mathbf{u}}_h \in V_h^2, \tag{5.2a}$$

$$\big(\boldsymbol{\mathcal{R}}_L \mathbf{u}_h, \mathbf{u}_h\big)_{\mu\times\varepsilon} = \|\mathbf{u}_h\|_{\mu\times\varepsilon}^2 - \frac{\tau^2}{4}\|\boldsymbol{\mathcal{C}}_{\mathbf{E}}^e \mathbf{E}_h\|_\mu^2 \quad \text{for } \mathbf{u}_h = (\mathbf{H}_h, \mathbf{E}_h) \in V_h^2. \tag{5.2b}$$

Next, we give an energy identity which allows us to prove the stability of (5.1a) under the following CFL condition:

$$\tau \le \frac{2\theta}{C_{\mathrm{bnd},c} c_{\infty,c}} \min_{K\in\mathcal{T}_{h,c}} h_K, \tag{5.3a}$$

where $0 < \theta < 1$ is a fixed parameter which satisfies

$$\widetilde{\theta} := \theta^2 + \alpha\theta < 1. \tag{5.3b}$$

Note that the CFL condition depends on the stabilization parameter α. For larger α we obtain a method with a stricter CFL condition.

Lemma 5.2. *The approximation* $\mathbf{u}_h^n = (\mathbf{H}_h^n, \mathbf{E}_h^n)$ *obtained from* (5.1a) *satisfies the energy identity*

(5.4)

$$\|\mathbf{u}_h^{n+1}\|_{\mu\times\varepsilon}^2 - \frac{\tau^2}{4}\|\boldsymbol{\mathcal{C}}_{\mathbf{E}}^e \mathbf{E}_h^{n+1}\|_\mu^2 - \alpha\frac{\tau}{2}|\mathbf{u}_h^{n+1}|_{\boldsymbol{\mathcal{S}}^e}^2 + \alpha\frac{\tau}{2}\sum_{m=0}^{n}|\mathbf{u}_h^{m+1}+\mathbf{u}_h^m|_{\boldsymbol{\mathcal{S}}^e}^2$$
$$= \|\mathbf{u}_h^0\|_{\mu\times\varepsilon}^2 - \frac{\tau^2}{4}\|\boldsymbol{\mathcal{C}}_{\mathbf{E}}^e \mathbf{E}_h^0\|_\mu^2 - \alpha\frac{\tau}{2}|\mathbf{u}_h^0|_{\boldsymbol{\mathcal{S}}^e}^2 + \frac{\tau}{2}\sum_{m=0}^{n}\big(\mathbf{j}_h^{m+1}+\mathbf{j}_h^m, \mathbf{u}_h^{m+1}+\mathbf{u}_h^m\big)_{\mu\times\varepsilon}.$$

If we assume that the CFL condition (5.3) *is satisfied, the following stability result holds true:*

$$(1-\widetilde{\theta})\|\mathbf{u}_h^{n+1}\|_{\mu\times\varepsilon}^2 + \alpha\frac{\tau}{2}\sum_{m=0}^{n}|\mathbf{u}_h^{m+1}+\mathbf{u}_h^m|_{\boldsymbol{\mathcal{S}}^e}^2 \leq e^{3/2}\left(\|\mathbf{u}^0\|_{\mu\times\varepsilon}^2 + \frac{T+1}{\delta(1-\widetilde{\theta})}\frac{\tau}{4}\sum_{m=0}^{n}\|\mathbf{J}^{m+1}+\mathbf{J}^m\|^2\right) \tag{5.5}$$

for $n = 1, 2, \ldots, N$.

Observe that the bound deteriorates for $\widetilde{\theta} \nearrow 1$.

Remark 5.3. In case of the central fluxes locally implicit scheme from [24] the CFL condition only requires the condition $\theta^2 < 1$. The additional term $\alpha\theta$ entering (5.3b) stems from the (explicit) integration of the stabilization operators.

Proof. We take the $\mu\times\varepsilon$-inner product of (5.1a) with $\mathbf{u}_h^{n+1}+\mathbf{u}_h^n$ and obtain

$$\big(\boldsymbol{\mathcal{R}}_L\mathbf{u}_h^{n+1} - \boldsymbol{\mathcal{R}}_R\mathbf{u}_h^n, \mathbf{u}_h^{n+1}+\mathbf{u}_h^n\big)_{\mu\times\varepsilon} = \big(-\tau\alpha\boldsymbol{\mathcal{S}}^e\mathbf{u}_h^n + \frac{\tau}{2}(\mathbf{j}_h^{n+1}+\mathbf{j}_h^n), \mathbf{u}_h^{n+1}+\mathbf{u}_h^n\big)_{\mu\times\varepsilon}.$$

The adjointness of $\boldsymbol{\mathcal{R}}_L$, $\boldsymbol{\mathcal{R}}_R$ from (5.2a) and furthermore (5.2b) imply

$$\big(\boldsymbol{\mathcal{R}}_L\mathbf{u}_h^{n+1} - \boldsymbol{\mathcal{R}}_R\mathbf{u}_h^n, \mathbf{u}_h^{n+1}+\mathbf{u}_h^n\big)_{\mu\times\varepsilon} = \|\mathbf{u}_h^{n+1}\|_{\mu\times\varepsilon}^2 - \|\mathbf{u}_h^n\|_{\mu\times\varepsilon}^2.$$

Thus, we conclude

(5.6)

$$\|\mathbf{u}_h^{n+1}\|_{\mu\times\varepsilon}^2 - \|\mathbf{u}_h^n\|_{\mu\times\varepsilon}^2 + \tau\alpha\big(\boldsymbol{\mathcal{S}}^e\mathbf{u}_h^n, \mathbf{u}_h^{n+1}+\mathbf{u}_h^n\big)_{\mu\times\varepsilon} = \frac{\tau}{2}\big(\mathbf{j}_h^{n+1}+\mathbf{j}_h^n, \mathbf{u}_h^{n+1}+\mathbf{u}_h^n\big)_{\mu\times\varepsilon}.$$

Moreover, we have that

$$\begin{aligned}\big(\boldsymbol{\mathcal{S}}^e\mathbf{u}_h^n, \mathbf{u}_h^{n+1}+\mathbf{u}_h^n\big)_{\mu\times\varepsilon} &= \Big(\frac{1}{2}\boldsymbol{\mathcal{S}}^e(\mathbf{u}_h^{n+1}+\mathbf{u}_h^n) - \frac{1}{2}\boldsymbol{\mathcal{S}}^e(\mathbf{u}_h^{n+1}-\mathbf{u}_h^n), \mathbf{u}_h^{n+1}+\mathbf{u}_h^n\Big)_{\mu\times\varepsilon}\\ &= \frac{1}{2}|\mathbf{u}_h^{n+1}+\mathbf{u}_h^n|_{\boldsymbol{\mathcal{S}}^e}^2 \quad - \frac{1}{2}\big(|\mathbf{u}_h^{n+1}|_{\boldsymbol{\mathcal{S}}^e}^2 - |\mathbf{u}_h^n|_{\boldsymbol{\mathcal{S}}^e}^2\big).\end{aligned}$$

Here, we used the definition of $|\cdot|_{\boldsymbol{\mathcal{S}}^e}$ and the symmetry of $\boldsymbol{\mathcal{S}}^e$ (see (4.22) and (4.20b)) for the second equality. Inserting this identity into (5.6) and summing yields the energy identity (5.4).

For the stability bound (5.5) we use the boundedness results for $\boldsymbol{\mathcal{C}}^e$ and $|\cdot|_{\boldsymbol{\mathcal{S}}^e}$ obtained in Theorem 4.7 in combination with the CFL condition (5.3) to infer

$$\begin{aligned}\frac{\tau^2}{4}\|\boldsymbol{\mathcal{C}}_{\mathbf{E}}^e\mathbf{E}_h^{n+1}\|_\mu^2 + \alpha\frac{\tau}{2}|\mathbf{u}_h^{n+1}|_{\boldsymbol{\mathcal{S}}^e}^2 &\leq \theta^2\|\mathbf{E}_h^{n+1}\|_\varepsilon^2 + \alpha\theta\|\mathbf{u}_h^{n+1}\|_{\mu\times\varepsilon}^2\\ &\leq \widetilde{\theta}\|\mathbf{u}_h^{n+1}\|_{\mu\times\varepsilon}^2.\end{aligned} \tag{5.7}$$

Here, we further used $\widehat{C}_{\mathrm{bnd},c} \le C_{\mathrm{bnd},c}$. Using this bound in (5.4) and, moreover, applying the Cauchy–Schwarz inequality and the weighted Young's inequality with weight $\gamma > 0$ gives

$$(1-\widetilde{\theta})\|\mathbf{u}_h^{n+1}\|_{\mu\times\varepsilon}^2 + \alpha\frac{\tau}{2}\sum_{m=0}^{n}|\mathbf{u}_h^{m+1}+\mathbf{u}_h^m|_{\boldsymbol{\mathcal{S}}^e}^2 \le \|\mathbf{u}_h^0\|_{\mu\times\varepsilon}^2 + \frac{\tau}{4\gamma}\sum_{m=0}^{n}\|\mathbf{j}_h^{m+1}+\mathbf{j}_h^m\|_{\mu\times\varepsilon}^2 + \gamma\frac{\tau}{2}\sum_{m=0}^{n}\big(\|\mathbf{u}_h^{m+1}\|_{\mu\times\varepsilon}^2 + \|\mathbf{u}_h^m\|_{\mu\times\varepsilon}^2\big).$$

We choose the weight $\gamma = (1-\widetilde{\theta})/(T+1)$, so that the discrete Gronwall lemma is applicable (Lemma A.1 with $\lambda = 1/(T+1)$). This yields the result. □

Besides the stability of our numerical scheme the energy identity (5.4) also implies that it is dissipative w.r.t. the following perturbed electromagnetic energy

$$\widetilde{\mathcal{E}}(\mathbf{H}_h,\mathbf{E}_h) = \mathcal{E}(\mathbf{H}_h,\mathbf{E}_h) - \frac{\tau^2}{8}\|\boldsymbol{\mathcal{C}}_{\mathbf{E}}^e\mathbf{E}_h\|_\mu^2 - \alpha\frac{\tau}{4}|\mathbf{u}_h|_{\boldsymbol{\mathcal{S}}^e}^2.$$

Indeed, we have that

$$\widetilde{\mathcal{E}}(\mathbf{H}_h^n,\mathbf{E}_h^n) = \widetilde{\mathcal{E}}(\mathbf{H}_h^0,\mathbf{E}_h^0) - \alpha\frac{\tau}{4}\sum_{m=0}^{n-1}|\mathbf{u}_h^{m+1}+\mathbf{u}_h^m|_{\boldsymbol{\mathcal{S}}^e}^2, \qquad n=1,2,\dots,N. \tag{5.8}$$

5.2. **Error analysis.** In this section we prove the convergence of the scheme (2.5) using an energy technique. The main result is stated in Theorem 5.10.

For the exact solution $\mathbf{u}^n = (\mathbf{H}^n,\mathbf{E}^n) = (\mathbf{H}(t_n),\mathbf{E}(t_n))$ of (2.1) at time t_n and its discretization $\mathbf{u}_h^n = (\mathbf{H}_h^n,\mathbf{E}_h^n) \approx \mathbf{u}^n$ given by (2.5) we introduce the full discretization error

$$\mathbf{e}^n = \mathbf{u}^n - \mathbf{u}_h^n = (\mathbf{e}_{\mathbf{H}}^n,\mathbf{e}_{\mathbf{E}}^n) = (\mathbf{H}^n-\mathbf{H}_h^n,\mathbf{E}^n-\mathbf{E}_h^n), \tag{5.9a}$$

and split it into

$$\mathbf{e}^n = \mathbf{e}_\pi^n - \mathbf{e}_h^n = (\mathbf{u}^n - \pi_h\mathbf{u}^n) - (\mathbf{u}_h^n - \pi_h\mathbf{u}^n). \tag{5.9b}$$

Assumption 4.6 implies that our mesh $\mathcal{T}_h$ has optimal polynomial approximation properties in the sense of [8, Definition 1.55]. Thus, for $\mathbf{H},\mathbf{E} \in H^{k+1}(K)^3$, $K \in \mathcal{T}_h$, $F \in \mathcal{F}_h$, $F \subset \partial K$, we have

$$\|\mathbf{e}_{\pi,\mathbf{H}}\|_{\mu,K} \le C_{\mathrm{app}}h_K^{k+1}|\mathbf{H}|_{k+1,K}, \qquad \|\mathbf{e}_{\pi,\mathbf{E}}\|_{\varepsilon,K} \le C_{\mathrm{app}}h_K^{k+1}|\mathbf{E}|_{k+1,K}, \tag{5.10a}$$

$$\|\mathbf{e}_{\pi,\mathbf{H}}\|_{\mu,F} \le \widehat{C}_{\mathrm{app}}h_K^{k+1/2}|\mathbf{H}|_{k+1,K}, \quad \|\mathbf{e}_{\pi,\mathbf{E}}\|_{\varepsilon,F} \le \widehat{C}_{\mathrm{app}}h_K^{k+1/2}|\mathbf{E}|_{k+1,K}, \tag{5.10b}$$

with constants C_{app}, $\widehat{C}_{\mathrm{app}}$ which depend on ρ but are independent of both the mesh element K and its size h_K; cf. [8, Lemmas 1.58, 1.59]. Thus it remains to examine $\mathbf{e}_h^n$.

5.2.1. *Error recursion.* In the next lemma we prove that the error $\mathbf{e}_h^n$ satisfies the recursion (5.1a) of the approximation $\mathbf{u}_h^n$ where the source term $\frac{\tau}{2}(\mathbf{j}_h^{n+1}+\mathbf{j}_h^n)$ is substituted by a defect.

Lemma 5.4. *Let* $\mathbf{u} \in C\big(0,T;V_\star\big) \cap C^3\big(0,T;L^2(\Omega)^6\big)$ *be the exact solution of* (2.1). *The error* $\mathbf{e}_h^n$ *definied in* (5.9b) *satisfies*

$$\boldsymbol{\mathcal{R}}_L\mathbf{e}_h^{n+1} = \boldsymbol{\mathcal{R}}_R\mathbf{e}_h^n - \tau\alpha\boldsymbol{\mathcal{S}}^e\mathbf{e}_h^n + \mathbf{d}^n, \qquad \mathbf{e}_h^0 = 0. \tag{5.11a}$$

The defect $\mathbf{d}^n = \mathbf{d}_\pi^n + \mathbf{d}_h^n$ *is given by*

$$\mathbf{d}_\pi^n = -\frac{\tau}{2}\boldsymbol{\mathcal{C}}\big(\mathbf{e}_\pi^{n+1} + \mathbf{e}_\pi^n\big) + \tau\alpha\boldsymbol{\mathcal{S}}^e\mathbf{e}_\pi^n - \frac{\tau^2}{4}\begin{pmatrix}0\\ \boldsymbol{\mathcal{C}}_{\mathbf{H}}^e\boldsymbol{\mathcal{C}}_{\mathbf{E}}\big(\mathbf{e}_{\pi,\mathbf{E}}^{n+1} - \mathbf{e}_{\pi,\mathbf{E}}^n\big)\end{pmatrix} \tag{5.11b}$$

and

$$\mathbf{d}_h^n = \tau^2\pi_h\delta^n - \frac{\tau^2}{4}\begin{pmatrix}0\\ \boldsymbol{\mathcal{C}}_{\mathbf{H}}^e\pi_h\Delta_{\mathbf{H}}^n\end{pmatrix}, \tag{5.11c}$$

where

$$\delta^n = \int_{t_n}^{t_{n+1}} \frac{(t-t_n)(t_{n+1}-t)}{2\tau^2}\partial_t^3\mathbf{u}(t)\,dt, \qquad \Delta_{\mathbf{H}}^n = \int_{t_n}^{t_{n+1}} \partial_t^2\mathbf{H}(t)\,dt. \tag{5.11d}$$

Proof. First, we observe that the recursion (5.1a) can be written as

$$\mathbf{u}_h^{n+1} - \mathbf{u}_h^n = \frac{\tau}{2}\boldsymbol{\mathcal{C}}\big(\mathbf{u}_h^{n+1} + \mathbf{u}_h^n\big) - \tau\alpha\boldsymbol{\mathcal{S}}^e\mathbf{u}_h^n + \frac{\tau}{2}(\mathbf{j}_h^{n+1} + \mathbf{j}_h^n) + \frac{\tau^2}{4}\begin{pmatrix}0\\ \boldsymbol{\mathcal{C}}_{\mathbf{H}}^e\boldsymbol{\mathcal{C}}_{\mathbf{E}}(\mathbf{E}_h^{n+1} - \mathbf{E}_h^n)\end{pmatrix}.$$

Next, we insert the projected exact solution into this recursion,

$$\begin{aligned}\pi_h(\mathbf{u}^{n+1} - \mathbf{u}^n) =& \frac{\tau}{2}\boldsymbol{\mathcal{C}}\pi_h\big(\mathbf{u}^{n+1} + \mathbf{u}^n\big) - \tau\alpha\boldsymbol{\mathcal{S}}^e\pi_h\mathbf{u}^n \\ &+ \frac{\tau}{2}(\mathbf{j}_h^{n+1} + \mathbf{j}_h^n) + \frac{\tau^2}{4}\begin{pmatrix}0\\ \boldsymbol{\mathcal{C}}_{\mathbf{H}}^e\boldsymbol{\mathcal{C}}_{\mathbf{E}}\pi_h(\mathbf{E}^{n+1} - \mathbf{E}^n)\end{pmatrix} - \mathbf{d}^n.\end{aligned} \tag{5.12}$$

Subtracting these two equations yields (5.11a). It remains to determine the defect $\mathbf{d}^n$. By using a Taylor expansion of $\mathbf{u}^{n+1/2}$ around t_n and around t_{n+1} we deduce that

$$\mathbf{u}^{n+1} - \mathbf{u}^n = \frac{\tau}{2}\big(\partial_t\mathbf{u}^{n+1} + \partial_t\mathbf{u}^n\big) - \tau^2\delta^n, \tag{5.13}$$

where the remainder is given in (5.11d). Projecting Maxwell's equations (3.2) onto V_h^2 and applying the consistency property (4.11) of the discrete curl-operators we obtain

$$\pi_h\partial_t\mathbf{u}(t) = \boldsymbol{\mathcal{C}}\mathbf{u}(t) + \mathbf{j}_h(t).$$

Using this identity and $\boldsymbol{\mathcal{S}}^e\mathbf{u}^n = 0$, which follows from the consistency of the explicit stabilization operators (4.19), the projection of (5.13) onto V_h^2 can be written as

$$\pi_h(\mathbf{u}^{n+1} - \mathbf{u}^n) = \frac{\tau}{2}\boldsymbol{\mathcal{C}}(\mathbf{u}^{n+1} + \mathbf{u}^n) - \tau\alpha\boldsymbol{\mathcal{S}}^e\mathbf{u}^n + \frac{\tau}{2}(\mathbf{j}_h^{n+1} + \mathbf{j}_h^n) - \tau^2\pi_h\delta^n. \tag{5.14}$$

Comparing (5.12) and (5.14) we infer

$$\mathbf{d}^n = -\frac{\tau}{2}\boldsymbol{\mathcal{C}}(\mathbf{e}_\pi^{n+1} + \mathbf{e}_\pi^n) + \tau\alpha\boldsymbol{\mathcal{S}}^e\mathbf{e}_\pi^n + \tau^2\pi_h\delta^n + \frac{\tau^2}{4}\begin{pmatrix}0\\ \boldsymbol{\mathcal{C}}_{\mathbf{H}}^e\boldsymbol{\mathcal{C}}_{\mathbf{E}}\pi_h(\mathbf{E}^{n+1} - \mathbf{E}^n)\end{pmatrix}.$$

As in [24, Proof of Lemma 5.1] one can show

$$\boldsymbol{\mathcal{C}}_{\mathbf{H}}^e\boldsymbol{\mathcal{C}}_{\mathbf{E}}\pi_h(\mathbf{E}^{n+1} - \mathbf{E}^n) = -\boldsymbol{\mathcal{C}}_{\mathbf{H}}^e\pi_h\Delta_{\mathbf{H}}^n - \boldsymbol{\mathcal{C}}_{\mathbf{H}}^e\boldsymbol{\mathcal{C}}_{\mathbf{E}}(\mathbf{e}_{\pi,\mathbf{E}}^{n+1} - \mathbf{e}_{\pi,\mathbf{E}}^n),$$

which finishes the proof. □

For the central fluxes case we pointed out in [24] that a naive convergence proof involving the recursion (5.11) only leads to an error bound of order 1.5. The problem lies in the defect $\frac{\tau^2}{4}\boldsymbol{\mathcal{C}}_{\mathbf{H}}^e\pi_h\Delta_{\mathbf{H}}^n$, which suffers from an order reduction from

τ^3 to $\tau^{2.5}$. This problem also occurs in the here considered uwpind fluxes case. In [24] we resolved this problem by splitting the quadrature defect $\mathbf{d}_h^n$ into

$$\mathbf{d}_h^n = \tau^2 \pi_h \delta^n + (\boldsymbol{\mathcal{R}}_L - \boldsymbol{\mathcal{R}}_R)\xi^n, \qquad \xi^n = \begin{pmatrix} \xi_{\mathbf{H}}^n \\ \xi_{\mathbf{E}}^n \end{pmatrix} = \frac{\tau}{4} \begin{pmatrix} \chi_e \pi_h \Delta_{\mathbf{H}}^n \\ 0 \end{pmatrix}. \tag{5.15}$$

Here, $(\boldsymbol{\mathcal{R}}_L - \boldsymbol{\mathcal{R}}_R)\xi^n$ contains the problematic defect $\frac{\tau^2}{4}\boldsymbol{\mathcal{C}}_{\mathbf{H}}^e \pi_h \Delta_{\mathbf{H}}^n$. Then, using this particular representation of the defect we could show that its contribution to the *global* error is of order two in time. However, the error analysis provided in [24] does not rely on an energy technique that is needed in the upwind fluxes case to show the improved spatial convergence order $k + 1/2$. Unfortunately, it turns out that even the energy technique applied directly to (5.11), (5.15) fails to give the desired temporal convergence order. The essential idea—besides the energy technique—is to consider a modified error $\widetilde{\mathbf{e}}_h^n$ instead of $\mathbf{e}_h^n$. A related idea has been presented in [32]. In the following lemma we introduce this modified error and give the associated error recursion.

Lemma 5.5. *Under the assumptions of Lemma* 5.4 *the modified error*

$$\widetilde{\mathbf{e}}_h^n = \mathbf{e}_h^n - \xi^{n-1}, \ n \geq 1, \qquad \widetilde{\mathbf{e}}_h^0 = \mathbf{e}_h^0 = 0, \tag{5.16a}$$

satisfies

$$\boldsymbol{\mathcal{R}}_L \widetilde{\mathbf{e}}_h^{n+1} = \boldsymbol{\mathcal{R}}_R \widetilde{\mathbf{e}}_h^n - \tau\alpha \boldsymbol{\mathcal{S}}^e \widetilde{\mathbf{e}}_h^n + \widetilde{\mathbf{d}}^n, \qquad n \geq 0, \tag{5.16b}$$

with defect

$$\widetilde{\mathbf{d}}^n = \begin{cases} \mathbf{d}_\pi^0 + \tau^2 \pi_h \delta^0 - \boldsymbol{\mathcal{R}}_R \xi^0, & n = 0, \\ \mathbf{d}_\pi^n + \tau^2 \pi_h \delta^n - \boldsymbol{\mathcal{R}}_R (\xi^n - \xi^{n-1}) - \tau\alpha \boldsymbol{\mathcal{S}}^e \xi^{n-1}, & n \geq 1. \end{cases} \tag{5.16c}$$

Moreover, if the CFL condition (5.3) *is satisfied, we have that*

$$\begin{aligned} (1 - \widetilde{\theta}) \|\widetilde{\mathbf{e}}_h^{n+1}\|_{\mu\times\varepsilon}^2 + \alpha \frac{\tau}{2} \sum_{m=0}^{n} |\widetilde{\mathbf{e}}_h^{m+1} + \widetilde{\mathbf{e}}_h^m|_{\boldsymbol{\mathcal{S}}^e}^2 \\ \leq \big(\widetilde{\mathbf{d}}^0, \widetilde{\mathbf{e}}_h^1\big)_{\mu\times\varepsilon} + \sum_{m=1}^{n} \big(\widetilde{\mathbf{d}}^m, \widetilde{\mathbf{e}}_h^{m+1} + \widetilde{\mathbf{e}}_h^m\big)_{\mu\times\varepsilon}. \end{aligned} \tag{5.17}$$

Since the indicator function χ_e is matched to the spatial mesh we have $\xi^n \in V_h^2$ and thus $\widetilde{\mathbf{e}}_h^n \in V_h^2$.

We observe that in (5.16c), except for $n = 0$, the problematic defect $(\boldsymbol{\mathcal{R}}_L - \boldsymbol{\mathcal{R}}_R)\xi^n$ could be replaced by the difference $\xi^n - \xi^{n-1}$. This allows us to gain an additional factor τ and to avoid an order reduction.

Proof. The error recursion (5.16a) follows by employing the splitting (5.15) of $\mathbf{d}_h^n$ in (5.11a).

The error $\widetilde{\mathbf{e}}_h^n$ satisfies the recursion (5.1a) of the locally implicit scheme with defect $\widetilde{\mathbf{d}}^n$ instead of the source terms. Hence, the energy identity Lemma 5.2 holds true for $\widetilde{\mathbf{e}}_h^n$. A computation analogous to (5.7) and the fact that $\widetilde{\mathbf{e}}_h^0 = 0$ yields the bound (5.17). □

5.3. **Bounds on defects.** It remains to bound the defects. This requires the following regularity on the exact solution $\mathbf{u} = (\mathbf{H}, \mathbf{E})$ of Maxwell's equations (2.1), which we assume for the remaining paper:

$$\begin{aligned} &\mathbf{u} \in C\big(0,T; D(\mathcal{C}) \cap H^{k+1}(\mathcal{T}_h)^6\big) \cap C^3\big(0,T; L^2(\Omega)^6\big), \\ &\mathbf{E} \in C^1\big(0,T; H^{k+1}(\mathcal{T}_{h,c})^3\big), \quad \mathbf{H} \in C^2\big(0,T; H^{\max(1,k-1)}(\mathcal{T}_{h,e})^3\big). \end{aligned} \tag{5.18}$$

Moreover, from now on we assume that the CFL condition (5.3) is satisfied with $\widetilde{\theta} \in (0,1)$, and that $n\tau \le T$. For the sake of readability we give the following bounds with respect to a generic constant C, which depends on $C_{\pi,c}$, $\widehat{C}_\pi$, C_{ctr}, $\widehat{C}_{\mathrm{app}}$, $C_{\mathrm{bnd},c}$ and $c_{\infty,c}$, but is independent of τ, h_K and α. Moreover, we introduce two weights $\gamma_1, \gamma_2 > 0$ which we will choose in our main Theorem 5.10.

We start with the projection defect $\mathbf{d}_\pi^n$.

Lemma 5.6. *For all $\varphi_h \in V_h^2$ we have the bound*

$$\begin{aligned} \big(\mathbf{d}_\pi^n, \varphi_h\big)_{\mu\times\varepsilon} &\le (1+\alpha^2)\gamma_1\tau|\varphi_h|_{\boldsymbol{\mathcal{S}}^e}^2 + 2\gamma_2\tau\|\varphi_h\|_{\mu\times\varepsilon}^2 \\ &\quad + \frac{C}{\gamma_1}\tau\Big(\big|\mathbf{u}^{n+1}+\mathbf{u}^n\big|_{k+1,\mathcal{T}_{h,c},2,k+\frac12}^2 + |\mathbf{u}^n|_{k+1,\mathcal{T}_{h,c},2,k+\frac12}^2\Big) \\ &\quad + \frac{C}{\gamma^2}\tau\Big(\big|\mathbf{u}^{n+1}+\mathbf{u}^n\big|_{k+1,\mathcal{T}_{h,i},2,k}^2 + \int_{t_n}^{t_{n+1}} |\partial_t\mathbf{E}(t)|_{k+1,\mathcal{T}_{h,c},2,k+\frac12}^2\ dt\Big). \end{aligned}$$

Proof. The first two terms of $\mathbf{d}_\pi^n$ are bounded by applying Young's inequality with weights γ_1, γ_2 to (4.29), (4.30). For the third term we use the Cauchy–Schwarz inequality and the weighted Young's inequality to obtain

$$\begin{aligned} \frac{\tau^2}{4}\left(\begin{pmatrix} 0 \\ \boldsymbol{\mathcal{C}}_{\mathbf{H}}^e\boldsymbol{\mathcal{C}}_{\mathbf{E}}\big(\mathbf{e}_{\pi,\mathbf{E}}^{n+1} - \mathbf{e}_{\pi,\mathbf{E}}^n\big)\end{pmatrix}, \varphi_h\right)_{\mu\times\varepsilon} &\le \gamma_2\tau\|\varphi_h\|_{\mu\times\varepsilon}^2 + \frac{C}{\gamma_2}\tau^3\|\boldsymbol{\mathcal{C}}_{\mathbf{H}}^e\boldsymbol{\mathcal{C}}_{\mathbf{E}}\big(\mathbf{e}_{\pi,\mathbf{E}}^{n+1} - \mathbf{e}_{\pi,\mathbf{E}}^n\big)\|_\varepsilon^2 \\ &\le \gamma_2\tau\|\varphi_h\|_{\mu\times\varepsilon}^2 + \frac{C}{\gamma_2}\tau\|\boldsymbol{\mathcal{C}}_{\mathbf{E}}^e\big(\mathbf{e}_{\pi,\mathbf{E}}^{n+1} - \mathbf{e}_{\pi,\mathbf{E}}^n\big)\|_\mu^2. \end{aligned} \tag{5.19}$$

Here, we used $\boldsymbol{\mathcal{C}}_{\mathbf{H}}^e\boldsymbol{\mathcal{C}}_{\mathbf{E}} = \boldsymbol{\mathcal{C}}_{\mathbf{H}}^e\boldsymbol{\mathcal{C}}_{\mathbf{E}}^e$, the boundedness result for $\boldsymbol{\mathcal{C}}_{\mathbf{H}}^e$ from Theorem 4.7, and the CFL condition (5.3) for the second inequality. Moreover, we have

$$\begin{aligned} \tau\|\boldsymbol{\mathcal{C}}_{\mathbf{E}}^e\big(\mathbf{e}_{\pi,\mathbf{E}}^{n+1} - \mathbf{e}_{\pi,\mathbf{E}}^n\big)\|_\mu^2 &\le \tau^2\int_{t_n}^{t_{n+1}} \|\boldsymbol{\mathcal{C}}_{\mathbf{E}}^e\partial_t\mathbf{e}_{\pi,\mathbf{E}}(t)\|_\mu^2\ dt \\ &\le C\tau\int_{t_n}^{t_{n+1}} |\partial_t\mathbf{E}(t)|_{k+1,\mathcal{T}_{h,c},2,k+\frac12}^2\ dt, \end{aligned}$$

where we used $\|\boldsymbol{\mathcal{C}}_{\mathbf{E}}^e\mathbf{e}_{\pi,\mathbf{E}}\|_\mu \le C|\mathbf{E}|_{k+1,\mathcal{T}_{h,c},2,k}$ (see [24, Equation (5.4b)]), and the CFL condition. ∎

Next, we address the defect $\boldsymbol{\mathcal{R}}_R(\xi^n - \xi^{n-1})$.

Lemma 5.7. *For all $\varphi_h \in V_h^2$ and all $n \ge 1$ we have*

$$\big(\boldsymbol{\mathcal{R}}_R(\xi^n - \xi^{n-1}), \varphi_h\big)_{\mu\times\varepsilon} \le \gamma_2\tau\|\varphi_h\|_{\mu\times\varepsilon}^2 + \frac{C}{\gamma_2}\tau^4\int_{t_{n-1}}^{t_{n+1}} \|\partial_t^3\mathbf{H}(t)\|_{\mu,\mathcal{T}_{h,c}}^2\ dt.$$

Proof. For dG functions $\mathbf{H}_h \in V_h$ and $\varphi_h = (\phi_h, \psi_h) \in V_h^2$ we have by the definitions of $\boldsymbol{\mathcal{R}}_L$ in (5.1b) and of $\boldsymbol{\mathcal{C}}^e_{\mathbf{H}}$ in (4.16) that

$$\begin{aligned}\left(\boldsymbol{\mathcal{R}}_R\begin{pmatrix}\chi_e\mathbf{H}_h\\0\end{pmatrix},\varphi_h\right)_{\mu\times\varepsilon} &= \big(\chi_e\mathbf{H}_h,\phi_h\big)_\mu + \frac{\tau}{2}\big(\boldsymbol{\mathcal{C}}^e_{\mathbf{H}}\mathbf{H}_h,\psi_h\big)_\varepsilon\\ &\le \gamma_2\tau\|\varphi_h\|^2_{\mu\times\varepsilon} + \frac{C}{\gamma_2\tau}\Big(\|\mathbf{H}_h\|^2_{\mu,\mathcal{T}_{h,e}} + \frac{\tau^2}{4}\|\boldsymbol{\mathcal{C}}^e_{\mathbf{H}}\mathbf{H}_h\|^2_\varepsilon\Big)\\ &\le \gamma_2\tau\|\varphi_h\|^2_{\mu\times\varepsilon} + \frac{C}{\gamma_2\tau}\|\mathbf{H}_h\|^2_{\mu,\mathcal{T}_{h,c}}. \qquad (5.20)\end{aligned}$$

Here, the first inequality is obtained by the Cauchy–Schwarz inequality and the weighted Young's inequality, and the second inequality follows from the boundedness result for $\boldsymbol{\mathcal{C}}^e_{\mathbf{H}}$, i.e., (4.27a), and the CFL condition (5.3). Using this, we have

$$\begin{aligned}\big(\boldsymbol{\mathcal{R}}_R(\xi^n-\xi^{n-1}),\varphi_h\big)_{\mu\times\varepsilon} &\le \gamma_2\tau\|\varphi_h\|^2_{\mu\times\varepsilon} + \frac{C}{\gamma_2\tau}\|\xi^n_{\mathbf{H}}-\xi^{n-1}_{\mathbf{H}}\|^2_\mu\\ &\le \gamma_2\tau\|\varphi_h\|^2_{\mu\times\varepsilon} + \frac{C\tau^4}{\gamma_2}\int_{t_{n-1}}^{t_{n+1}}\|\partial_t^3\mathbf{H}(t)\|^2_{\mu,\mathcal{T}_{h,c}}\,dt.\end{aligned}$$

Here, the second inequality follows via a Taylor expansion of $\partial_t\mathbf{H}^{m+1}$ around t_m and around t_{m+2}, which yields

$$\begin{aligned}\xi^n_{\mathbf{H}}-\xi^{n-1}_{\mathbf{H}} &= \frac{\tau}{4}\chi_e\pi_h\big(\partial_t\mathbf{H}^{n+1}-2\partial_t\mathbf{H}^n+\partial_t\mathbf{H}^{n-1}\big)\\ &= \frac{\tau^2}{4}\int_{t_{n-1}}^{t_{n+1}}\left(1-\frac{|t_n-t|}{\tau}\right)\chi_e\pi_h\big(\partial_t^3\mathbf{H}(t)\big)\,dt.\end{aligned}$$

This finishes the proof. □

In the subsequent lemma we provide a bound on $\tau\alpha\boldsymbol{\mathcal{S}}^e\xi^{n-1}$.

Lemma 5.8. *For all $\varphi_h \in V_h^2$ and all $n \ge 1$ the following bound holds:*

$$\begin{aligned}\big(\tau\alpha\boldsymbol{\mathcal{S}}^e\xi^{n-1},\varphi_h\big)_{\mu\times\varepsilon} \le{}& \gamma_1\alpha^2\tau|\varphi_h|^2_{\boldsymbol{\mathcal{S}}}\\ &+\frac{C}{\gamma_1}\tau^4\int_{t_{n-1}}^{t_n}\|\mu\partial_t^2\mathbf{H}(t)\|^2_{1,\mathcal{T}_{h,e}}\,dt\\ &+\frac{C}{\gamma_1}\int_{t_{n-1}}^{t_n}|\partial_t^2\mathbf{H}(t)|^2_{\max(1,k-1),\mathcal{T}_{h,e},2,k+\frac12}\,dt.\end{aligned}$$

Proof. By using the Cauchy–Schwarz inequality and Young's inequality we obtain

$$\tau\alpha\big(\boldsymbol{\mathcal{S}}^e\xi^{n-1},\varphi_h\big)_{\mu\times\varepsilon} \le \tau\alpha|\xi^{n-1}|_{\boldsymbol{\mathcal{S}}^e}|\varphi_h|_{\boldsymbol{\mathcal{S}}^e} \le \gamma_1\alpha^2\tau|\varphi_h|^2_{\boldsymbol{\mathcal{S}}^e} + \frac{C\tau^3}{\gamma_1}|\chi_e\pi_h\Delta^{n-1}_{\mathbf{H}}|^2_{\boldsymbol{\mathcal{S}}^e_{\mathbf{H}}}.$$

In the second term we decompose $\pi_h\Delta^{n-1}_{\mathbf{H}} = \Delta^{n-1}_{\mathbf{H}} - \Delta^{n-1}_{\pi}$, where

$$\Delta^{n-1}_{\mathbf{H}} = \int_{t_{n-1}}^{t_n}\partial_t^2\mathbf{H}(t)\,dt, \qquad \Delta^{n-1}_{\pi} = \int_{t_{n-1}}^{t_n}\partial_t^2\mathbf{e}_{\pi,\mathbf{H}}(t)\,dt\,.$$

By the definition of $|\cdot|_{\boldsymbol{\mathcal{S}}_{\mathbf{H}}^e}$ in (4.21a) we have

$$\begin{aligned}\frac{\tau^3}{\gamma_1}|\chi_e\pi_h\Delta_{\mathbf{H}}^{n-1}|^2_{\boldsymbol{\mathcal{S}}_{\mathbf{H}}^e} &= \frac{\tau^3}{\gamma_1}\sum_{F\in\mathcal{F}_{h,c}^{\mathrm{int}}} a_F\|n_F\times[\![\chi_e\pi_h\Delta_{\mathbf{H}}^{n-1}]\!]_F\|_F^2\\ &\le \frac{C\tau^3}{\gamma_1}\sum_{F\in\mathcal{F}_{h,c}^{\mathrm{int}}} a_F\Big(\|[\![\chi_e\Delta_{\mathbf{H}}^{n-1}]\!]_F\|_F^2+\|[\![\chi_e\Delta_{\pi}^{n-1}]\!]_F\|_F^2\Big).\end{aligned}\tag{5.21}$$

Here, the inequality is obtained via the splitting of $\pi_h\Delta_{\mathbf{H}}^{n-1}$, the triangle inequality, Young's inequality, and $|n_F|=1$. We bound the two terms separately. For the subsequent calculations it is important to recall that the set $\mathcal{F}_{h,c}^{\mathrm{int}}$ only contains faces bordering coarse elements. So, for the remaining proof let $F\in\mathcal{F}_{h,c}^{\mathrm{int}}$, which yields $K,K_F\in\mathcal{T}_{h,c}$.

(a) For the first term the Cauchy–Schwarz inequality in L^2 yields

$$\begin{aligned}a_F\|[\![\chi_e\Delta_{\mathbf{H}}^{n-1}]\!]_F\|_F^2 &\le a_F\tau\int_{t_{n-1}}^{t_n}\|[\![\chi_e\partial_t^2\mathbf{H}(t)]\!]_F\|_F^2\,dt\\ &\le Ca_F\tau\int_{t_{n-1}}^{t_n}\mu_K^{-1}\|\chi_e(\mu\partial_t^2\mathbf{H}(t))\|_{1,K}^2\,dt\\ &\quad+Ca_F\tau\int_{t_{n-1}}^{t_n}\mu_{K_F}^{-1}\|\chi_e(\mu\partial_t^2\mathbf{H}(t))\|_{1,K_F}^2\,dt\\ &\le C\tau\int_{t_{n-1}}^{t_n}\|\chi_e(\mu\partial_t^2\mathbf{H}(t))\|_{1,K\cup K_F}^2\,dt.\end{aligned}$$

Here, we used the triangle inequality, Young's inequality and the continuous trace inequality [8, Section 1.1.3] for the second inequality, and

$$a_F\le c_K\mu_K,\qquad a_F\le c_{K_F}\mu_{K_F}\tag{5.22}$$

for the third inequality.

(b) For the second term we have

$$\begin{aligned}a_F\|[\![\chi_e\Delta_{\pi}^{n-1}]\!]_F\|_F^2 &\le a_F\tau\int_{t_{n-1}}^{t_n}\|[\![\chi_e\partial_t^2\mathbf{e}_{\pi,\mathbf{H}}(t)]\!]_F\|_F^2\,dt\\ &\le C\tau\int_{t_{n-1}}^{t_n}\|\chi_e\partial_t^2\mathbf{e}_{\pi,\mathbf{H}}(t)|_K\|_{\mu,F}^2+\|\chi_e\partial_t^2\mathbf{e}_{\pi,\mathbf{H}}(t)|_{K_F}\|_{\mu,F}^2\,dt,\end{aligned}$$

where the second inequality is obtained via the triangle inequality, Young's inequality and (5.22). Let $\widetilde{k}=\max(1,k-1)$, then the regularity assumptions on $\partial_t^2\mathbf{H}$ together with (5.10b) imply

$$\|\partial_t^2\mathbf{e}_{\pi,\mathbf{H}}|_K\|_{\mu,F}^2\le Ch_K^{2\widetilde{k}-1}|\partial_t^2\mathbf{H}|_{\widetilde{k},K}^2\le C\tau^{-4}h_K^{2\widetilde{k}+3}|\partial_t^2\mathbf{H}|_{\widetilde{k},K}^2.$$

For the last inequality we used the CFL condition (5.3). Hence, we end up with

$$a_F\|[\![\chi_e\Delta_{\pi}^{n-1}]\!]_F\|_F^2\le C\tau^{-3}\int_{t_{n-1}}^{t_n}h_K^{2k+1}|\chi_e\partial_t^2\mathbf{H}(t)|_{\widetilde{k},K}^2+h_{K_F}^{2k+1}|\chi_e\partial_t^2\mathbf{H}(t)|_{\widetilde{k},K_F}^2\,dt,$$

where we used $h_K^{2\widetilde{k}+3}\le h_K^{2k+1}$. (In the case $k>1$ this bound holds true for all h_K. For $k=1$ it is true for $h_K\le 1$, i.e., the relevant case for a convergence proof. If one wants to include the case $h_K>1$ an additional constant $\mathrm{vol}_d(\Omega)^2$ has to be included in this bound.)

Inserting the results from (a) and (b) in (5.21) yields the desired bound. □

It remains to establish a bound on $\widetilde{\mathbf{d}}^0$.

Lemma 5.9. *We have the bound*

$$\begin{aligned}(1-\theta^2)\big(\widetilde{\mathbf{d}}^0,\widetilde{\mathbf{e}}_h^1\big)_{\mu\times\varepsilon} \le & C|\mathbf{u}^1+\mathbf{u}^0|^2_{k+1,\mathcal{T}_h,2,k+1}\\ &+C\tau^4\max_{t\in[0,\tau]}\|\partial_t^2\mathbf{H}(t)\|^2_{\mu,\mathcal{T}_{h,e}}+C\tau^4\int_0^\tau\|\partial_t^3\mathbf{u}(t)\|^2_{\mu\times\varepsilon}\,dt\\ &+C\tau\left|\mathbf{u}^0\right|^2_{k+1,\mathcal{T}_{h,c},2,k+\frac12}+C\tau\left|\mathbf{u}^1-\mathbf{u}^0\right|^2_{k+1,\mathcal{T}_{h,c},2,k+\frac12}.\end{aligned}$$

Proof. This proof needs the following two results shown in [24, Lemma 4.1,4.2]: Under the CFL condition (5.3) the operator $\boldsymbol{\mathcal{R}}_L$ is invertible and we have the following bounds:

$$\|\boldsymbol{\mathcal{R}}_L^{-1}\|_{\mu\times\varepsilon}\le\frac{1}{1-\theta^2},\qquad \|(\boldsymbol{\mathcal{R}}_L^{-1}\boldsymbol{\mathcal{R}}_R)^m\|_{\mu\times\varepsilon}\le\frac{1}{\sqrt{1-\theta^2}}. \tag{5.23}$$

By (5.16b), $\widetilde{\mathbf{e}}_h^0=0$ and subsequently (5.2b) we have

$$\big(\widetilde{\mathbf{d}}^0,\widetilde{\mathbf{e}}_h^1\big)_{\mu\times\varepsilon}=\big(\boldsymbol{\mathcal{R}}_L\widetilde{\mathbf{e}}_h^1,\widetilde{\mathbf{e}}_h^1\big)_{\mu\times\varepsilon}\le\|\widetilde{\mathbf{e}}_h^1\|^2_{\mu\times\varepsilon}.$$

From (5.16b) we obtain

$$\widetilde{\mathbf{e}}_h^1=\boldsymbol{\mathcal{R}}_L^{-1}(\mathbf{d}_\pi^0+\mathbf{d}_h^0)+\boldsymbol{\mathcal{R}}_L^{-1}\boldsymbol{\mathcal{R}}_R\xi^0.$$

Using $\boldsymbol{\mathcal{R}}_L-\boldsymbol{\mathcal{R}}_R=-\frac{\tau}{2}\boldsymbol{\mathcal{C}}$ and (4.16) we can write

$$\mathbf{d}_\pi^0=\frac12(\boldsymbol{\mathcal{R}}_L-\boldsymbol{\mathcal{R}}_R)(\mathbf{e}_\pi^1+\mathbf{e}_\pi^0)+\tau\alpha\boldsymbol{\mathcal{S}}^e\mathbf{e}_\pi^0+\frac{\tau}{4}(\boldsymbol{\mathcal{R}}_L-\boldsymbol{\mathcal{R}}_R)\begin{pmatrix}\boldsymbol{\mathcal{C}}^e_{\mathbf{E}}(\mathbf{e}^1_{\pi,\mathbf{E}}-\mathbf{e}^0_{\pi,\mathbf{E}})\\0\end{pmatrix}.$$

Using the bounds (5.23) we infer

$$\begin{aligned}(1-\theta^2)\|\widetilde{\mathbf{e}}_h^1\|_{\mu\times\varepsilon}\le & C\big(\|\xi^0\|_{\mu\times\varepsilon}+\|\delta^0\|_{\mu\times\varepsilon}\big)\\ &+C\big(\tau\|\boldsymbol{\mathcal{S}}^e\mathbf{e}_\pi^0\|_{\mu\times\varepsilon}+\|\mathbf{e}_\pi^1+\mathbf{e}_\pi^0\|_{\mu\times\varepsilon}+\tau\|\boldsymbol{\mathcal{C}}^e_{\mathbf{E}}(\mathbf{e}^1_{\pi,\mathbf{E}}-\mathbf{e}^0_{\pi,\mathbf{E}})\|_\mu\big).\end{aligned}$$

The bound on the first two terms are clear. The fourth term can be bounded with (5.10a) and the last one as in the proof of Lemma 5.6. For the remaining defect we use (4.30) and subsequently (4.28) and the CFL condition

$$\begin{aligned}\tau\big(\boldsymbol{\mathcal{S}}^e\mathbf{e}_\pi,\varphi_h\big)_{\mu\times\varepsilon}&\le C_{\pi,c}\tau|\varphi_h|_{\boldsymbol{\mathcal{S}}^e}|u|_{k+1,\mathcal{T}_{h,c},2,k+\frac12}\\ &\le C_{\pi,c}(\widehat{C}_{\mathrm{bnd},c}c_{\infty,c})^{1/2}\tau\|\varphi_h\|_{\mu\times\varepsilon,\mathcal{T}_{h,e}\cup\mathcal{T}_{h,ci},2,-1/2}|u|_{k+1,\mathcal{T}_{h,c},2,k+\frac12}\\ &\le\sqrt{2}C_{\pi,c}\tau^{1/2}\|\varphi_h\|_{\mu\times\varepsilon}|u|_{k+1,\mathcal{T}_{h,c},2,k+\frac12}.\end{aligned}$$

As a consequence, we have

$$\tau\|\boldsymbol{\mathcal{S}}^e\mathbf{e}_\pi^0\|_{\mu\times\varepsilon}\le C\tau^{1/2}|u^0|_{k+1,\mathcal{T}_{h,c},2,k+\frac12}.$$

This concludes the proof. □

5.4. **Main result.** Using the stability results and the bounds on the defects, we now have all ingredients to show our main result.

Theorem 5.10. *Assume that the exact solution* $\mathbf{u} = (\mathbf{H}, \mathbf{E})$ *of Maxwell's equations* (2.1) *satisfies*

$$\mathbf{u} \in C\big(0,T; D(\mathcal{C}) \cap H^{k+1}(\mathcal{T}_h)^6\big) \cap C^3\big(0,T; L^2(\Omega)^6\big),$$
$$\mathbf{E} \in C^1\big(0,T; H^{k+1}(\mathcal{T}_{h,c})^3\big), \quad \mathbf{H} \in C^2\big(0,T; H^{\max(1,k-1)}(\mathcal{T}_{h,e})^3\big).$$

Moreover, assume that the CFL condition (5.3) *is satisfied with* $\widetilde{\theta} \in (0,1)$*, and assume that* $n\tau \le T$*. Then, the error of the upwind fluxes locally implicit scheme* (2.5) *is bounded by*

$$\begin{aligned}
\|\mathbf{u}^n - \mathbf{u}_h^n\|_{\mu\times\varepsilon}^2 + \alpha\frac{\tau}{4}\sum_{m=0}^{n-1} |\widetilde{\mathbf{e}}_h^{m+1} + \widetilde{\mathbf{e}}_h^m|_{\boldsymbol{\mathcal{S}}^e}^2 \\
&\le C'|\mathbf{u}^n + \mathbf{u}^1 + \mathbf{u}^0|_{k+1,\mathcal{T}_h,1,k+1}^2 + C'\tau^4 \max_{t\in[0,t_n]} \|\partial_t^2\mathbf{H}(t)\|_{\mu,\mathcal{T}_{h,e}}^2 \\
&\quad + C'\tau^4 \int_0^{t_n} \|\partial_t^3\mathbf{u}(t)\|_{\mu\times\varepsilon}^2 + \|\mu\partial_t^2\mathbf{H}(t)\|_{1,\mathcal{T}_{h,e}}^2\, dt \\
&\quad + C'\tau \sum_{m=0}^{n} \Big(|\mathbf{u}^m|_{k+1,\mathcal{T}_{h,c},2,k+\frac12}^2 + |\mathbf{u}^m|_{k+1,\mathcal{T}_{h,i},2,k}^2 \Big) \\
&\quad + C' \int_0^{t_n} |\partial_t\mathbf{E}(t)|_{k+1,\mathcal{T}_{h,c},2,k+\frac12}^2 + |\partial_t^2\mathbf{H}(t)|_{\max(1,k-1),\mathcal{T}_{h,e},2,k+\frac12}^2\, dt \\
&\le C''\Big(\max_{K\in\mathcal{T}_{h,e}} h_K^{2k+1} + \max_{K\in\mathcal{T}_{h,i}} h_K^{2k} + \tau^4 \Big).
\end{aligned}$$

The constant C' *has the dependencies of* C *and additional involves* $1/(1-\widetilde{\theta})$ *and* $(1+\alpha^2)/\alpha$*. The constant* C'' *depends on* C' *and on* $|\mathbf{u}(t)|_{k+1,\mathcal{T}_h}$*,* $|\partial_t\mathbf{E}(t)|_{k+1,\mathcal{T}_{h,c}}$*,* $|\partial_t^2\mathbf{H}(t)|_{\max(1,k-1),\mathcal{T}_{h,e}}$*,* $\|\partial_t^2\mathbf{H}(t)\|_\mu$*, and* $\|\partial_t^3\mathbf{u}(t)\|_{\mu\times\varepsilon}$*,* $t \in [0,t_n]$*.*

Remark 5.11. We recall from Remark 4.9 that by choosing degree $k+1$ on the (very few) elements in $\mathcal{T}_{h,c} \cap \mathcal{T}_{h,i}$, we obtain the convergence rate

$$\|\mathbf{u}^n - \mathbf{u}_h^n\|_{\mu\times\varepsilon}^2 + \alpha\frac{\tau}{4}\sum_{m=0}^{n-1} |\widetilde{\mathbf{e}}_h^{m+1} + \widetilde{\mathbf{e}}_h^m|_{\boldsymbol{\mathcal{S}}^e}^2 \le C''\Big(\max_{K\in\mathcal{T}_{h,c}} h_K^{2k+1} + \max_{K\in\mathcal{T}_{h,f}} h_K^{2k} + \tau^4 \Big).$$

This is the desired rate $k+1/2$ on the coarse elements and k on the fine elements.

Proof. The full discretization error is given by $\mathbf{e}^n = \mathbf{e}_\pi^n - \widetilde{\mathbf{e}}_h^n - \xi^{n-1}$. Using $\big(\mathbf{e}_\pi, \varphi_h\big)_{\mu\times\varepsilon} = 0$, and the triangle inequality and Young's inequality we infer

$$\|\mathbf{e}^n\|_{\mu\times\varepsilon}^2 \le \|\mathbf{e}_\pi^n\|_{\mu\times\varepsilon}^2 + 2\|\widetilde{\mathbf{e}}_h^n\|_{\mu\times\varepsilon}^2 + 2\|\xi^{n-1}\|_{\mu\times\varepsilon}^2.$$

The first and the last term can be bounded by

$$\|\mathbf{e}_\pi^n\|_{\mu\times\varepsilon}^2 \le C_{\mathrm{app}}^2|\mathbf{u}|_{k+1,\mathcal{T}_h,2,k+1}, \qquad \|\xi^{n-1}\|_{\mu\times\varepsilon}^2 \le C\tau^4 \max_{t\in[t_{n-1},t_n]} \|\partial_t^2\mathbf{H}(t)\|_{\mu,\mathcal{T}_{h,e}}^2,$$

where the first bound stems from (5.10a). For the remaining error $\widetilde{\mathbf{e}}_h^n$ we have the bound (5.17) and inserting

$$\big(\mathbf{d}_h^n, \varphi_h\big)_{\mu\times\varepsilon} \le \gamma_2\tau\|\varphi_h\|_{\mu\times\varepsilon}^2 + \frac{C}{\gamma_2}\tau^4 \int_{t_n}^{t_{n+1}} \|\partial_t^3\mathbf{u}(t)\|_{\mu\times\varepsilon}^2\, dt,$$

and the results from Lemmas 5.6–5.9 with $\gamma_1 = \alpha/2(1+2\alpha^2)$ we obtain

$$\begin{aligned}(1-\widetilde{\theta})\|\widetilde{\mathbf{e}}_h^{n+1}\|_{\mu\times\varepsilon}^2 + \alpha\frac{\tau}{4}\sum_{m=0}^{n}|\widetilde{\mathbf{e}}_h^{m+1}+\widetilde{\mathbf{e}}_h^{m}|_{\boldsymbol{\mathcal{S}}^e}^2 \\ \le 3\gamma_2\tau\sum_{m=1}^{n}\|\widetilde{\mathbf{e}}_h^{m+1}+\widetilde{\mathbf{e}}_h^{m}\|_{\mu\times\varepsilon}^2 \\ + C|\mathbf{u}^1+\mathbf{u}^0|_{k+1,\mathcal{T}_h,2,k+1}^2 + \tau^4\max_{t\in[0,\tau]}\|\partial_t^2\mathbf{H}(t)\|_{\mu,\mathcal{T}_{h,c}}^2 \\ + C'\tau\sum_{m=0}^{n}\left|\mathbf{u}^{m+1}+\mathbf{u}^m\right|_{k+1,\mathcal{T}_{h,i},2,k}^2 \\ + C'\tau\sum_{m=0}^{n}\left|\mathbf{u}^{m+1}+2\mathbf{u}^m\right|_{k+1,\mathcal{T}_{h,c},2,k+\frac{1}{2}}^2 \\ + C\gamma_2\int_0^{t_{n+1}}\tau^4\|\partial_t^3\mathbf{u}(t)\|_{\mu\times\varepsilon}^2 + |\partial_t\mathbf{E}(t)|_{k+1,\mathcal{T}_{h,c},2,k+\frac{1}{2}}^2\,dt \\ + C'\int_0^{t_n}\tau^4\|\mu\partial_t^2\mathbf{H}(t)\|_{1,\mathcal{T}_{h,e}}^2 + |\partial_t^2\mathbf{H}(t)|_{\max(1,k-1),\mathcal{T}_{h,e},2,k+\frac{1}{2}}^2\,dt.\end{aligned}$$

By the triangle inequality, Young's inequality and by choosing the weight $\gamma_2 = \frac{1-\widetilde{\theta}}{12(T+1)}$ we have

$$3\gamma_2\tau\|\widetilde{\mathbf{e}}_h^{m+1}+\widetilde{\mathbf{e}}_h^{m}\|_{\mu\times\varepsilon}^2 \le \frac{1-\widetilde{\theta}}{T+1}\frac{\tau}{2}\big(\|\widetilde{\mathbf{e}}_h^{m+1}\|_{\mu\times\varepsilon}^2 + \|\widetilde{\mathbf{e}}_h^{m}\|_{\mu\times\varepsilon}^2\big).$$

Finally, applying the discrete Gronwall Lemma A.1 yields the result. □

6. Implementation issues and numerical results

We conclude this paper by sketching the efficient implementation of the locally implicit method and presenting some numerical experiments confirming our theoretical results. Details on the implementation and a series of additional examples can be found in [31].

6.1. **Implementation.** At first glance (5.1) seems to require the solution of a linear system of all degrees of freedom (dof) of $\mathbf{u}_h = (\mathbf{H}_h, \mathbf{E}_h)$ in every time step. However, we can reduce this system by using a Schur decomposition. This yields the equivalent linear system

$$\begin{pmatrix}\boldsymbol{\mathcal{I}} & \frac{\tau}{2}\boldsymbol{\mathcal{C}}_{\mathbf{E}} \\ 0 & \boldsymbol{\mathcal{L}}\end{pmatrix}\begin{pmatrix}\mathbf{H}_h^{n+1}\\ \mathbf{E}_h^{n+1}\end{pmatrix} = \begin{pmatrix}\mathbf{b}_{\mathbf{H}}^n \\ \mathbf{b}_{\mathbf{E}}^n + \frac{\tau}{2}\boldsymbol{\mathcal{C}}_{\mathbf{H}}\mathbf{b}_{\mathbf{H}}^n\end{pmatrix}, \tag{6.1a}$$

where the right-hand side reads

$$\mathbf{b}_{\mathbf{H}}^n = \mathbf{H}_h^n - \frac{\tau}{2}\boldsymbol{\mathcal{C}}_{\mathbf{E}}\mathbf{E}_h^n - \tau\alpha\boldsymbol{\mathcal{S}}_{\mathbf{H}}^e\mathbf{H}_h^n, \tag{6.1b}$$

$$\mathbf{b}_{\mathbf{E}}^n = \mathbf{E}_h^n + \frac{\tau}{2}\boldsymbol{\mathcal{C}}_{\mathbf{H}}\mathbf{H}_h^n - \frac{\tau^2}{4}\boldsymbol{\mathcal{C}}_{\mathbf{H}}^e\boldsymbol{\mathcal{C}}_{\mathbf{E}}\mathbf{E}_h^n - \tau\alpha\boldsymbol{\mathcal{S}}_{\mathbf{E}}^e\mathbf{E}_h^n - \frac{\tau}{2}\big(\mathbf{J}_h^{n+1}+\mathbf{J}_h^n\big), \tag{6.1c}$$

and where the Schur complement is given by

$$\boldsymbol{\mathcal{L}} = \boldsymbol{\mathcal{I}} - \frac{\tau^2}{4}\boldsymbol{\mathcal{C}}_{\mathbf{H}}^e\boldsymbol{\mathcal{C}}_{\mathbf{E}} + \frac{\tau^2}{4}\boldsymbol{\mathcal{C}}_{\mathbf{H}}\boldsymbol{\mathcal{C}}_{\mathbf{E}} = \boldsymbol{\mathcal{I}} + \frac{\tau^2}{4}\boldsymbol{\mathcal{C}}_{\mathbf{H}}^i\boldsymbol{\mathcal{C}}_{\mathbf{E}}. \tag{6.1d}$$

Note that we have $\mathbf{H}_h^{n+1/2} = \mathbf{b}_{\mathbf{H}}^n + \frac{\tau}{2}\alpha\boldsymbol{\mathcal{S}}_{\mathbf{H}}^e\mathbf{H}_h^n$, and thus

$$\begin{aligned}\mathbf{b}_{\mathbf{E}}^n + \frac{\tau}{2}\boldsymbol{\mathcal{C}}_{\mathbf{H}}\mathbf{b}_{\mathbf{H}}^n &= \mathbf{E}_h^n - \tau\alpha\boldsymbol{\mathcal{S}}_{\mathbf{E}}^e\mathbf{E}_h^n \\ &\quad + \tau\boldsymbol{\mathcal{C}}_{\mathbf{H}}^e\mathbf{H}_h^{n+1/2} + \frac{\tau}{2}\boldsymbol{\mathcal{C}}_{\mathbf{H}}^i\big(\mathbf{H}_h^{n+1/2} + \mathbf{H}_h^n - \frac{\tau}{2}\boldsymbol{\mathcal{S}}_{\mathbf{H}}^e\mathbf{H}_h^n\big) - \frac{\tau}{2}\big(\mathbf{J}_h^{n+1} + \mathbf{J}_h^n\big).\end{aligned} \tag{6.2}$$

We summarize the computations needed to perform the time step from $\mathbf{u}_h^n$ to $\mathbf{u}_h^{n+1}$ with the locally implicit method in Algorithm 6.1.

Algorithm 6.1. Locally implicit method

Given $\mathbf{H}_h^n$, $\mathbf{E}_h^n$:

1: Compute $\mathbf{H}_h^{n+1/2} = \mathbf{b}_{\mathbf{H}}^n + \frac{\tau}{2}\alpha\boldsymbol{\mathcal{S}}_{\mathbf{H}}^e\mathbf{H}_h^n$ by (6.1b)

2: Compute $\mathbf{b}_{\mathbf{E}}^n + \frac{\tau}{2}\boldsymbol{\mathcal{C}}_{\mathbf{H}}\mathbf{b}_{\mathbf{H}}^n$ by (6.2)

3: Solve $\boldsymbol{\mathcal{L}}\mathbf{E}_h^{n+1} = \mathbf{b}_{\mathbf{E}}^n + \frac{\tau}{2}\boldsymbol{\mathcal{C}}_{\mathbf{H}}\mathbf{b}_{\mathbf{H}}^n$ with $\boldsymbol{\mathcal{L}}$ given in (6.1d)

4: Update $\mathbf{H}_h^{n+1} = \mathbf{H}_h^{n+1/2} - \frac{\tau}{2}\boldsymbol{\mathcal{C}}_{\mathbf{E}}\mathbf{E}_h^{n+1} - \frac{\tau}{2}\alpha\boldsymbol{\mathcal{S}}_{\mathbf{H}}^e\mathbf{H}_h^n$

The main effort of Algorithm 6.1 lies in Step 3, where a linear system with $\boldsymbol{\mathcal{L}}$ has to be solved. The efficiency of the locally implicit scheme now arises from the fact that $\boldsymbol{\mathcal{L}}$ involves $\boldsymbol{\mathcal{C}}_{\mathbf{H}}^i\boldsymbol{\mathcal{C}}_{\mathbf{E}}$ (rather than $\boldsymbol{\mathcal{C}}_{\mathbf{H}}\boldsymbol{\mathcal{C}}_{\mathbf{E}}$ as it would be for the fully implicit Crank–Nicolson method). Ordering the dof such that we first number the explicit mesh elements which only have explicit neighbors (the vast majority of elements) and then the remaining elements (the implicit elements and their neighbors) the matrix associated with the operator $\boldsymbol{\mathcal{L}}$ takes the form

$$\boldsymbol{\mathcal{L}} \longrightarrow \begin{pmatrix} I & 0 \\ 0 & * \end{pmatrix}.$$

The large identity block corresponds to the dofs resulting from the explicitly treated elements while the (tiny) lower right block corresponds to the implicitly treated elements. Thus, solving a linear system with $\boldsymbol{\mathcal{L}}$ is cheap and Step 3 in Algorithm 6.1 can be carried out almost as fast as the update of $\mathbf{E}_h^{n+1}$ with the explicit Verlet method (where $\boldsymbol{\mathcal{L}} = \boldsymbol{\mathcal{I}}$). For further details we refer to [31, Section 6.2].

6.2. **Numerical experiments.** For our numerical experiments we consider the transverse magnetic (TM) polarization of Maxwell's equations in a homogeneous medium with $\mu = \varepsilon = 1$ in the square $\Omega = (-1,1)^2 \subset \mathbb{R}^2$,

$$\begin{aligned}\partial_t\mathbf{H}_x(t) &= -\partial_y\mathbf{E}_z(t), \\ \partial_t\mathbf{H}_y(t) &= \partial_x\mathbf{E}_z(t), \\ \partial_t\mathbf{E}_z(t) &= -\partial_y\mathbf{H}_x(t) + \partial_x\mathbf{H}_y(t) - \mathbf{J}_z(t), \\ \mathbf{H}_x(0) &= \mathbf{H}_x^0, \quad \mathbf{H}_y(0) = \mathbf{H}_y^0, \quad \mathbf{E}_z(0) = \mathbf{E}_z^0.\end{aligned} \tag{6.3}$$

We choose $\mathbf{J}_z$ such that

$$\begin{aligned}\mathbf{H}_x(t) &= -\pi\sin(\pi x)\cos(\pi y)\exp(t), \\ \mathbf{H}_y(t) &= \pi\cos(\pi x)\sin(\pi y)\exp(t), \\ \mathbf{E}_z(t) &= \sin(\pi x)\sin(\pi y)\exp(t),\end{aligned} \tag{6.4a}$$

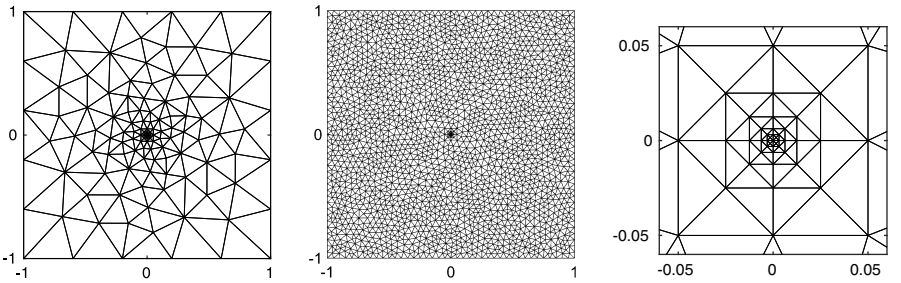

(a) Mesh level $\mathcal{T}_h^{(1)}$. (b) Mesh level $\mathcal{T}_h^{(4)}$. (c) Refinement of the elements in $[-0.05, 0.05]^2$.

FIGURE 2. Illustration of the meshes.

is a solution of (6.3), i.e.,

$$\mathbf{J}_z(t) = -(1+2\pi^2)\sin(\pi x)\sin(\pi y)\exp(t). \tag{6.4b}$$

As an example for locally refined grids we use the mesh sequence $\mathcal{T}_h^{(j)} = \mathcal{T}_h^{(j,4)}$, $1 \le j \le 4$, from [24, Section 6]. For the sake of briefness we only give a plot of the meshes $\mathcal{T}_h^{(1)}$, $\mathcal{T}_h^{(4)}$ and their refined part in Figure 2. The details on the meshes such as the element diameters, refinement factors, the decomposition of the mesh into explicitly and implicitly treated elements can be found in [24, Section 6].

As a reference time integrator we use the Verlet method with a full stabilization on the current iterates $\mathbf{H}_h^n$, $\mathbf{E}_h^n$. As already pointed out in Section 5 this scheme can be obtained from the locally implicit scheme (2.5) by choosing $\mathcal{T}_{h,e} = \mathcal{T}_h$. In fact, its recursion can be gained from (2.5) by changing $\boldsymbol{\mathcal{C}}_{\mathbf{H}}^e$, $\boldsymbol{\mathcal{C}}_{\mathbf{H}}^i$, $\boldsymbol{\mathcal{S}}_{\mathbf{H}}^e$ and $\boldsymbol{\mathcal{S}}_{\mathbf{E}}^e$ into $\boldsymbol{\mathcal{C}}_{\mathbf{H}}$, $\mathbf{0}$, $\boldsymbol{\mathcal{S}}_{\mathbf{H}}$ and $\boldsymbol{\mathcal{S}}_{\mathbf{E}}$, respectively. For all following results we ran our simulation until the final time $t_N = T = 1$ and its error $\mathbf{e}^N = \mathbf{u}^N - \mathbf{u}_h^N$ is always measured in the $L^2(\Omega)$ norm.

For a detailed discussion of the dependence of the CFL condition on the implicitly and explicitly treated parts of the mesh we refer to [24], since it makes no difference if we consider central or upwind fluxes. A new effect occurring for an upwind fluxes space discretization is the dependence of the maximal stable time step and of the error on the stabilization parameter α. We also refer to [11] for a related discussion of such effects when working with (fully explicit) low-storage Runge–Kutta schemes. The fact that the maximal stable time step is subject to α is seen from the condition (5.3b). The dependence of the error on α follows since the constant C' in Theorem 5.10 involves a factor $(1+\alpha^2)/\alpha$. Thus, for larger α we have two competing effects: on the one hand, the error constant gets smaller and on the other hand the CFL condition gets stricter. So, the optimal choice might be $\alpha \in (0,1)$ instead of $\alpha = 1$ (depending on the application). We validate both effects with the mesh $\mathcal{T}_h^{(1)}$. The maximal stable time step sizes we observe in our simulation are given in Figure 3a for the locally implicit scheme and in Figure 3b for the Verlet method. First of all, the results highlight the superior CFL condition of the locally implicit method compared to the Verlet method. Moreover, they confirm that a larger α or a higher polynomial degree (this dependence enters the CFL condition through the constant $C_{\mathrm{bnd},c}$) require a smaller time step in order

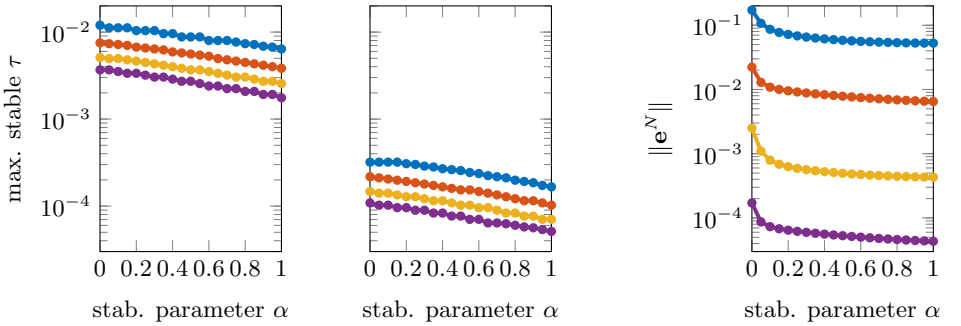

(a) Maximum stable time step τ for the locally implicit method.

(b) Maximum stable time step τ for the Verlet method.

(c) Error of the locally implicit scheme for time step size $\tau = 5 \cdot 10^{-4}$ and final time $t_N = T = 1$.

FIGURE 3. Dependence of the maximal stable time step and the error, respectively, on the stabilization parameter α. We used the mesh $\mathcal{T}_h^{(1)}$ and polynomial degrees $k = 2$ (blue), $k = 3$ (orange), $k = 4$ (yellow), $k = 5$ (purple).

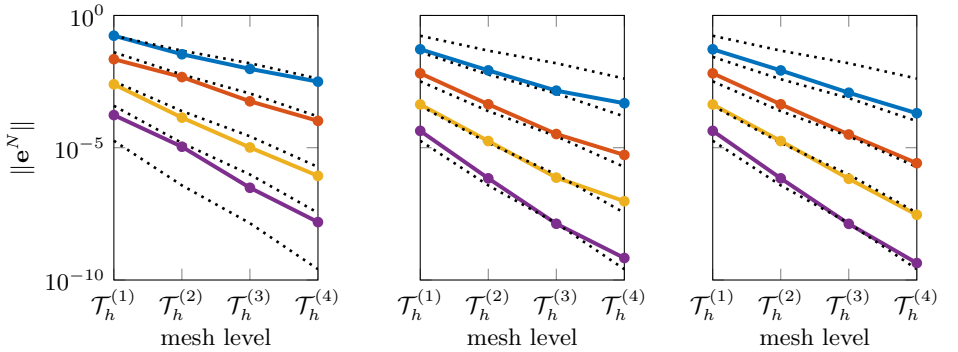

(a) Error of the locally implicit method with $\alpha = 0$ (central fluxes).

(b) Error of the locally implicit method with $\alpha = 1$ (upwind fluxes).

(c) Error of the Verlet method with $\alpha = 1$ (upwind fluxes).

FIGURE 4. Spatial convergence. As final time we used $t_N = T = 1$ and as time step $\tau = 10^{-5}$. We employed the polynomial degrees $k = 2$ (blue), $k = 3$ (orange), $k = 4$ (yellow), $k = 5$ (purple). The black dotted lines have slope $\max_{K \in \mathcal{T}_h} h_K^k$ for $k = 2, \ldots, 6$.

to ensure stability. Figure 3c depicts the correlation between the error (for a small time step $\tau = 5 \cdot 10^{-4}$) and the stabilization parameter α. We confirm that for larger α the error becomes smaller.

Next, we examine the spatial convergence. For this purpose we use a tiny time step size $\tau = 10^{-5}$ which is chosen small enough such that the spatial error dominates over the time discretization error. We give the results in Figures 4a and 4b for the locally implicit method with $\alpha = 0$ (central fluxes; see also Figure 2 from [24])

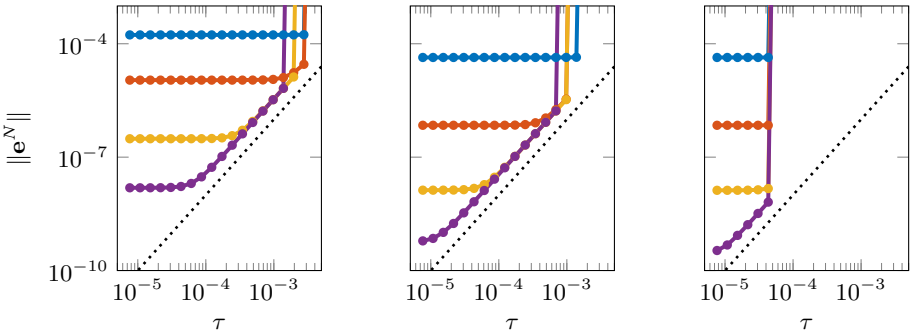

(a) Error of the locally implicit method with $\alpha = 0$ (central fluxes).

(b) Error of the locally implicit method with $\alpha = 1$ (upwind fluxes).

(c) Error of the Verlet method with $\alpha = 1$ (upwind fluxes).

FIGURE 5. Temporal convergence. We used the final time $t_N = T = 1$ and the polynomial degree $k = 5$. Moreover, we used the meshes $\mathcal{T}_h^{(1)}$ (blue), $\mathcal{T}_h^{(2)}$ (orange), $\mathcal{T}_h^{(3)}$ (yellow), and $\mathcal{T}_h^{(4)}$ (purple).

and with $\alpha = 1$ (full upwind fluxes), respectively. We clearly observe the superior convergence rate of the upwind fluxes scheme compared to the central fluxes case. In fact, we even observe a higher convergence rate $k+1$ for the stabilized method compared to $k+1/2$ given in Theorem 5.10. This behavior is well known [19]. The convergence rate in the central fluxes is k as predicted in [24]. As comparison we plotted in Figure 4c the error of the Verlet method with full upwind fluxes, i.e., with stabilization parameter $\alpha = 1$. We observe that the Verlet method shows the convergence rate $k+1$ for all mesh levels $\mathcal{T}_h^{(1)}, \dots, \mathcal{T}_h^{(4)}$. For the locally implicit method we observe the same rate for $\mathcal{T}_h^{(1)}, \dots, \mathcal{T}_h^{(3)}$ and then a slight decrease in the rate for $\mathcal{T}_h^{(4)}$. This confirms the spatial rate $\max_{K\in\mathcal{T}_{h,e}} h_K^{k+1/2} + \max_{K\in\mathcal{T}_{h,i}} h_K^k$ given in Theorem 5.10: For the meshes $\mathcal{T}_h^{(1)}, \dots, \mathcal{T}_h^{(3)}$ the implicitly treated part of the grid only consists of elements with a smaller diameter compared to those of the explicitly treated part; see [24, Table 1]. Thus, the spatial error is dominated by $\max_{K\in\mathcal{T}_{h,e}} h_K^{k+1/2}$ which we observe in the figure. Contrary, for the mesh $\mathcal{T}_h^{(4)}$ there are implicitly treated elements with a larger diameter than those in the explicitly treated part. Consequently, we also observe the rate $\max_{K\in\mathcal{T}_{h,i}} h_K^k$ in the spatial error.

Last, we verify the temporal convergence. For that purpose we use the polynomial degree $k = 5$ since for this degree, at least for larger time step sizes, the time integration error dominates the spatial error. The graphs of the errors of the locally implicit scheme are given in Figure 5a and Figure 5b for $\alpha = 0$ (see also Figure 3a from [24]) and for $\alpha = 1$, respectively. We clearly observe that both methods converge with order two in the time step which substantiates the order given in Theorem 5.10 and in [24, Theorem 5.3] for $\alpha = 1$ and $\alpha = 0$, respectively. Furthermore, we again observe the slightly weaker CFL condition in the case $\alpha = 0$ (this method is stable for a larger time step size; see also Figure 3a) and the superior space discretization error for $\alpha = 1$ (the plateaus indicating the space discretization errors are at a smaller size for this method, compare also Figure 3c). As an additional comparison we give in Figure 5c the errors we observe for the

Verlet method with $\alpha = 1$. This figure shows well that both the locally implicit scheme and the Verlet method are of the same temporal convergence order, i.e., of order two. Moreover, it again illustrates the considerably improved CFL condition of the locally implicit method compared to the Verlet method.

Appendix A. Gronwall inequalities

Lemma A.1 ((Modified) discrete Gronwall lemma)**.** *Let $\lambda \geq 0$, $\tau > 0$ and $\lambda\tau \leq \frac{3}{2}$. Furthermore, let a_n, b_n, $c_n \in \mathbb{R}$ such that $a_0 \leq b_0$, $b_n \leq b_{n+1}$, $c_n \geq 0$, and*

$$a_{n+1} + c_{n+1} \leq b_{n+1} + \lambda\frac{\tau}{2}\sum_{m=0}^{n}(a_{m+1} + a_m), \qquad n \geq 0. \tag{A.1}$$

Then we have $a_n + c_n \leq e^{\frac{3}{2}\lambda n\tau} b_n$, $n \geq 0$.

Proof. Since $c_n \geq 0$ we obtain from (A.1),

$$a_{n+1} + c_{n+1} \leq b_{n+1} + \lambda\frac{\tau}{2}\sum_{m=0}^{n}(a_{m+1} + c_{m+1} + a_m + c_m),$$

whence the statement follows from [14, Proposition 4.1] and $(1+x)/(1-x) \leq e^{3x}$ for $x \in [0, 3/4]$. □

Appendix B. Proofs postponed from Section 4

Proof of (4.28) *from Theorem* 4.7. For $\mathbf{u}_h = (\mathbf{H}_h, \mathbf{E}_h)$ we have $|\mathbf{u}_h|^2_{\boldsymbol{\mathcal{S}}^e} = |\mathbf{H}_h|^2_{\boldsymbol{\mathcal{S}}^e_{\mathbf{H}}} + |\mathbf{E}_h|^2_{\boldsymbol{\mathcal{S}}^e_{\mathbf{E}}}$, where by Definition 4.5,

$$|\mathbf{H}_h|^2_{\boldsymbol{\mathcal{S}}^e_{\mathbf{H}}} = \sum_{F\in\mathcal{F}^{\mathrm{int}}_{h,c}} a_F \|n_F \times [\![\mathbf{H}_h]\!]_F\|^2_F. \tag{B.1}$$

By $|n_F| = 1$, the triangle inequality, Young's inequality and the trace inequality (4.25) on the coarse mesh $\mathcal{T}_{h,c}$ we infer

$$\begin{aligned} a_F\|n_F \times [\![\mathbf{H}_h]\!]_F\|^2_F &\leq 2C^2_{\mathrm{tr},c} a_F \left(\varepsilon_K c_K^2 h_K^{-1}\|\mathbf{H}_h\|^2_{\mu,K} + \varepsilon_{K_F} c^2_{K_F} h^{-1}_{K_F}\|\mathbf{H}_h\|^2_{\mu,K_F}\right) \\ &\leq 2C^2_{\mathrm{tr},c} c_{\infty,c}\left(h_K^{-1}\|\mathbf{H}_h\|^2_{\mu,K} + h^{-1}_{K_F}\|\mathbf{H}_h\|^2_{\mu,K_F}\right), \end{aligned}$$

where the second inequality is obtained via

$$a_F\varepsilon_K c_K \leq 1, \qquad a_F\varepsilon_{K_F} c_{K_F} \leq 1, \tag{B.2}$$

Inserting this bound into (B.1) gives

$$|\mathbf{H}_h|^2_{\boldsymbol{\mathcal{S}}_{\mathbf{H}}} \leq \widehat{C}_{\mathrm{bnd},c} c_{\infty,c}\|\mathbf{H}_h\|^2_{\mu,\mathcal{T}_{h,c},2,-\frac{1}{2}}.$$

The proof of the bound for $|\mathbf{E}_h|^2_{\boldsymbol{\mathcal{S}}_{\mathbf{E}}}$ is done analogously. □

Proof of Theorem 4.8 . This proof is done in four steps.

(a) We start with the proof of (4.29): For $\mathbf{e}_\pi = (\mathbf{e}_{\pi,\mathbf{H}}, \mathbf{e}_{\pi,\mathbf{E}})$ and $\varphi_h = (\phi_h, \psi_h)$ we have

$$\left(\boldsymbol{\mathcal{C}}\mathbf{e}_\pi, \varphi_h\right)_{\mu\times\varepsilon} = \left(\boldsymbol{\mathcal{C}}_{\mathbf{E}}\mathbf{e}_{\pi,\mathbf{E}}, \phi_h\right)_\mu + \left(\boldsymbol{\mathcal{C}}_{\mathbf{H}}\mathbf{e}_{\pi,\mathbf{H}}, \psi_h\right)_\varepsilon. \tag{B.3}$$

By the partial integration formular (4.12b) for $\boldsymbol{\mathcal{C}}_{\mathbf{E}}$ and because the projection error $\mathbf{e}_{\pi,\mathbf{E}}$ is orthogonal to V_h (see (4.6)), we have

$$\begin{aligned}\big(\boldsymbol{\mathcal{C}}_{\mathbf{E}}\mathbf{e}_{\pi,\mathbf{E}},\phi_h\big)_\mu &= \sum_{F\in\mathcal{F}_h^{\mathrm{int}}} \big(n_F\times[\![\phi_h]\!]_F,\{\!\{\mathbf{e}_{\pi,\mathbf{E}}\}\!\}_F^{\varepsilon c}\big)_F\\ &\le \sum_{F\in\mathcal{F}_{h,c}^{\mathrm{int}}} \|n_F\times[\![\phi_h]\!]_F\|_F\;\|\{\!\{\mathbf{e}_{\pi,\mathbf{E}}\}\!\}_F^{\varepsilon c}\|_F\\ &\quad+\sum_{F\in\mathcal{F}_{h,i}^{\mathrm{int}}} \|n_F\times[\![\phi_h]\!]_F\|_F\;\|\{\!\{\mathbf{e}_{\pi,\mathbf{E}}\}\!\}_F^{\varepsilon c}\|_F.\end{aligned}\tag{B.4}$$

Here, we used the splitting of the mesh faces $\mathcal{F}_h^{\mathrm{int}}=\mathcal{F}_{h,c}^{\mathrm{int}}\,\dot\cup\,\mathcal{F}_{h,i}^{\mathrm{int}}$ from (4.15) and the Cauchy–Schwarz inequality. Using (4.7) we have

$$\begin{aligned}\|\{\!\{\mathbf{e}_{\pi,\mathbf{E}}\}\!\}_F^{\varepsilon c}\|_F^2 &= a_F^2\,\|\varepsilon_K c_K\mathbf{e}_{\pi,\mathbf{E}}|_K+\varepsilon_{K_F}c_{K_F}\mathbf{e}_{\pi,\mathbf{E}}|_{K_F}\|_F^2\\ &\le 2a_F^2\left(\|\varepsilon_K c_K\mathbf{e}_{\pi,\mathbf{E}}|_K\|_F^2+\|\varepsilon_{K_F}c_{K_F}\mathbf{e}_{\pi,\mathbf{E}}|_{K_F}\|_F^2\right)\\ &= 2a_F^2\left(\varepsilon_K c_K^2\|\mathbf{e}_{\pi,\mathbf{E}}|_K\|_{\varepsilon,F}^2+\varepsilon_{K_F}c_{K_F}^2\|\mathbf{e}_{\pi,\mathbf{E}}|_{K_F}\|_{\varepsilon,F}^2\right)\\ &\le 2a_F\left(c_K\|\mathbf{e}_{\pi,\mathbf{E}}|_K\|_{\varepsilon,F}^2+c_{K_F}\|\mathbf{e}_{\pi,\mathbf{E}}|_{K_F}\|_{\varepsilon,F}^2\right)\\ &\le 2a_F\,\widehat{C}_{\mathrm{app}}^2\left(c_K h_K^{2k+1}|\mathbf{E}|_{k+1,K}^2+c_{K_F}h_{K_F}^{2k+1}|\mathbf{E}|_{k+1,K_F}^2\right).\end{aligned}\tag{B.5}$$

Here, we applied the triangle inequality, Young's inequality, and (B.2). From now on, the two sums in (B.4) have to be treated differently.

(b) By the Cauchy–Schwarz inequality in $\mathbb{R}^{\mathrm{card}(\mathcal{F}_{h,c}^{\mathrm{int}})}$ with weight a_F, we obtain

$$\begin{aligned}&\sum_{F\in\mathcal{F}_{h,c}^{\mathrm{int}}} \|n_F\times[\![\phi_h]\!]_F\|_F\;\|\{\!\{\mathbf{e}_{\pi,\mathbf{E}}\}\!\}_F^{\varepsilon c}\|_F\\ &\quad\le\Big(\sum_{F\in\mathcal{F}_{h,c}^{\mathrm{int}}} a_F\|n_F\times[\![\phi_h]\!]_F\|_F^2\Big)^{1/2}\Big(\sum_{F\in\mathcal{F}_{h,c}^{\mathrm{int}}} a_F^{-1}\|\{\!\{\mathbf{e}_{\pi,\mathbf{E}}\}\!\}_F^{\varepsilon c}\|_F^2\Big)^{1/2}\\ &\quad\le\sqrt{2}\widehat{C}_{\mathrm{app}}|\phi_h|_{\boldsymbol{\mathcal{S}}_{\mathbf{H}}^{\varepsilon}}\Big(\sum_{F\in\mathcal{F}_{h,c}^{\mathrm{int}}} c_K h_K^{2k+1}|\mathbf{E}|_{k+1,K}^2+c_{K_F}h_{K_F}^{2k+1}|\mathbf{E}|_{k+1,K_F}^2\Big)^{1/2}\\ &\quad\le(2N_\partial c_{\infty,c})^{1/2}\widehat{C}_{\mathrm{app}}|\phi_h|_{\boldsymbol{\mathcal{S}}_{\mathbf{H}}^{\varepsilon}}|\mathbf{E}|_{k+1,\mathcal{T}_{h,e}\cup\mathcal{T}_{h,ci},2,k+1/2}.\end{aligned}\tag{B.6}$$

For the second inequality we used the Definition 4.5 of the stabilization seminorm and (B.5).

(c) Again the Cauchy–Schwarz inequality in $\mathbb{R}^{\mathrm{card}(\mathcal{F}_{h,i}^{\mathrm{int}})}$ implies

$$\begin{aligned}&\sum_{F\in\mathcal{F}_{h,i}^{\mathrm{int}}} \|n_F\times[\![\phi_h]\!]_F\|_F\;\|\{\!\{\mathbf{e}_{\pi,\mathbf{E}}\}\!\}_F^{\varepsilon c}\|_F\\ &\quad\le\Big(\sum_{F\in\mathcal{F}_{h,i}^{\mathrm{int}}} \omega_F\|n_F\times[\![\phi_h]\!]_F\|_F^2\Big)^{1/2}\Big(\sum_{F\in\mathcal{F}_{h,i}^{\mathrm{int}}} \omega_F^{-1}\|\{\!\{\mathbf{e}_{\pi,\mathbf{E}}\}\!\}_F^{\varepsilon c}\|_F^2\Big)^{1/2},\end{aligned}$$

where we choose the weight $\omega_F=a_F(h_K+h_{K_F})/2$. From the shape- and contact-regularity of the mesh $\mathcal{T}_h$, in fact by using (4.23), we deduce

$$\rho^{-1}a_F\le\omega_F h_K^{-1},\ \omega_F h_{K_F}^{-1}\le\rho a_F.\tag{B.7}$$

By $|n_F| = 1$, the triangle inequality, Young's inequality, and subsequently the trace inequality (4.25), we infer

$$\begin{aligned}\omega_F\|n_F \times [\![\phi_h]\!]_F\|_F^2 &\le 2\omega_F\big(\|\phi_h|_K\|_F^2 + \|\phi_h|_{K_F}\|_F^2\big)\\ &\le 2C_{\mathrm{tr}}^2\omega_F\big(h_K^{-1}\|\phi_h\|_K^2 + h_{K_F}^{-1}\|\phi_h\|_{K_F}^2\big)\\ &= 2C_{\mathrm{tr}}^2\omega_F\big(\mu_K^{-1}h_K^{-1}\|\phi_h\|_{\mu,K}^2 + \mu_{K_F}^{-1}h_{K_F}^{-1}\|\phi_h\|_{\mu,K_F}^2\big)\\ &\le 2C_{\mathrm{tr}}^2\rho a_F\big(\mu_K^{-1}\|\phi_h\|_{\mu,K}^2 + \mu_{K_F}^{-1}\|\phi_h\|_{\mu,K_F}^2\big)\\ &\le 2C_{\mathrm{tr}}^2\rho c_\infty\|\phi_h\|_{\mu,K\cup K_F}^2. \qquad \text{(B.8)}\end{aligned}$$

Here, the third inequality was obtained via (B.7) and the last inequality follows by (5.22). Last, we deduce from (B.5) with the aid of (B.7), that we have

$$\omega_F^{-1}\|\{\!\{\mathbf{e}_{\pi,\mathbf{E}}\}\!\}_F^{\varepsilon c}\|_F^2 \le 2\widehat{C}_{\mathrm{app}}^2\rho c_\infty\left(h_K^{2k}|\mathbf{E}|_{k+1,K}^2 + h_{K_F}^{2k}|\mathbf{E}|_{k+1,K_F}^2\right).$$

This yields

$$\sum_{F\in\mathcal{F}_{h,i}^{\mathrm{int}}}\|n_F \times [\![\phi_h]\!]_F\|_F\ \|\{\!\{\mathbf{e}_{\pi,\mathbf{E}}\}\!\}_F^{\varepsilon c}\|_F \le \widehat{C}_\pi\|\phi_h\|_{\mu,\mathcal{T}_{h,i}}|\mathbf{E}|_{k+1,\mathcal{T}_{h,i},2,k}. \qquad \text{(B.9)}$$

Inserting (B.6) and (B.9) into (B.4), we finally obtain

$$\big(\boldsymbol{\mathcal{C}}_{\mathbf{E}}\mathbf{e}_{\pi,\mathbf{E}},\phi_h\big)_\mu \le C_{\pi,c}|\phi_h|_{\boldsymbol{\mathcal{S}}_{\mathbf{H}}^e}|\mathbf{E}|_{k+1,\mathcal{T}_{h,e}\cup\mathcal{T}_{h,ci},2,k+1/2} + \widehat{C}_\pi\|\phi_h\|_{\mu,\mathcal{T}_{h,i}}|\mathbf{E}|_{k+1,\mathcal{T}_{h,i},2,k}.$$

Analogous computations show that

$$\big(\boldsymbol{\mathcal{C}}_{\mathbf{H}}\mathbf{e}_{\pi,\mathbf{H}},\psi_h\big)_\varepsilon \le C_{\pi,c}|\psi_h|_{\boldsymbol{\mathcal{S}}_{\mathbf{E}}^e}|\mathbf{H}|_{k+1,\mathcal{T}_{h,e}\cup\mathcal{T}_{h,ci},2,k+1/2} + \widehat{C}_\pi\|\psi_h\|_{\varepsilon,\mathcal{T}_{h,i}}|\mathbf{H}|_{k+1,\mathcal{T}_{h,i},2,k},$$

whence the bound (4.29) follows by (B.3) and the Cauchy–Schwarz inequality in $\mathbb{R}^2$.

(d) We proceed with proving the bound (4.30): By Definition 4.4, the Cauchy–Schwarz inequalities in $L^2(F)$ and in $\mathbb{R}^{\mathrm{card}(\mathcal{F}_{h,c}^{\mathrm{int}})}$ we have

$$\big(\boldsymbol{\mathcal{S}}_{\mathbf{H}}^e\mathbf{e}_{\pi,\mathbf{H}},\phi_h\big)_\mu \le |\phi_h|_{\boldsymbol{\mathcal{S}}_{\mathbf{H}}^e}\left(\sum_{F\in\mathcal{F}_{h,c}^{\mathrm{int}}}a_F\|n_F \times [\![\mathbf{e}_{\pi,\mathbf{H}}]\!]_F\|_F^2\right)^{1/2}.$$

By $|n_F| = 1$, the triangle inequality and Young's inequality we infer

$$\begin{aligned}a_F\|n_F \times [\![\mathbf{e}_{\pi,\mathbf{H}}]\!]_F\|_F^2 &\le 2a_F\big(\|\mathbf{e}_{\pi,\mathbf{H}}|_K\|_F^2 + \|\mathbf{e}_{\pi,\mathbf{H}}|_{K_F}\|_F^2\big)\\ &= 2a_F\big(\mu_K^{-1}\|\mathbf{e}_{\pi,\mathbf{H}}|_K\|_{\mu,F}^2 + \mu_{K_F}^{-1}\|\mathbf{e}_{\pi,\mathbf{H}}|_{K_F}\|_{\mu,F}^2\big)\\ &\le 2\widehat{C}_{\mathrm{app}}^2\big(c_K h_K^{2k+1}|\mathbf{H}|_{k+1,K}^2 + c_{K_F}h_{K_F}^{2k+1}|\mathbf{H}|_{k+1,K_F}^2\big).\end{aligned}$$

Here, the last inequality follows from (5.10b) and (5.22). Consequently, we have

$$\big(\boldsymbol{\mathcal{S}}_{\mathbf{H}}^e\mathbf{e}_{\pi,\mathbf{H}},\phi_h\big) \le C_{\pi,c}|\phi_h|_{\boldsymbol{\mathcal{S}}_{\mathbf{H}}}|\mathbf{H}|_{k+1,\mathcal{T}_{h,e}\cup\mathcal{T}_{h,ci},2,k+1/2},$$

and analogously we obtain

$$\big(\boldsymbol{\mathcal{S}}_{\mathbf{E}}^e\mathbf{e}_{\pi,\mathbf{E}},\psi_h\big) \le C_{\pi,c}|\psi_h|_{\boldsymbol{\mathcal{S}}_{\mathbf{E}}}|\mathbf{E}|_{k+1,\mathcal{T}_{h,e}\cup\mathcal{T}_{h,ci},2,k+1/2}.$$

Finally, by the Cauchy–Schwarz inequality in $\mathbb{R}^2$ we get the desired bound (4.30). □

References

[1] M. Almquist and M. Mehlin, *Multilevel local time-stepping methods of Runge-Kutta-type for wave equations*, SIAM J. Sci. Comput. **39** (2017), no. 5, A2020–A2048, DOI 10.1137/16M1084407. MR3697168

[2] J. Alvarez, L.D. Angulo, M.R. Cabello, A. Rubio Bretones, and S.G. Garcia, *An analysis of the leap-frog discontinuous Galerkin method for Maxwell's equations*, Microwave Theory and Techniques, IEEE Transactions on **62** (2014), no. 2, 197–207.

[3] K. Busch, M. König, and J. Niegemann, *Discontinuous Galerkin methods in nanophotonics*, Laser & Photonics Reviews **5** (2011), no. 6, 773–809.

[4] A. Demirel, J. Niegemann, K. Busch, and M. Hochbruck, *Efficient multiple time-stepping algorithms of higher order*, J. Comput. Phys. **285** (2015), 133–148, DOI 10.1016/j.jcp.2015.01.018. MR3306326

[5] S. Descombes, S. Lanteri, and L. Moya, *Locally implicit time integration strategies in a discontinuous Galerkin method for Maxwell's equations*, J. Sci. Comput. **56** (2013), no. 1, 190–218, DOI 10.1007/s10915-012-9669-5. MR3049948

[6] S. Descombes, S. Lanteri, and L. Moya, *Locally implicit discontinuous Galerkin time domain method for electromagnetic wave propagation in dispersive media applied to numerical dosimetry in biological tissues*, SIAM J. Sci. Comput. **38** (2016), no. 5, A2611–A2633. MR3543158

[7] S. Descombes, S. Lanteri, and L. Moya, *Temporal convergence analysis of a locally implicit discontinuous Galerkin time domain method for electromagnetic wave propagation in dispersive media*, J. Comput. Appl. Math. **316** (2017), 122–132, DOI 10.1016/j.cam.2016.09.038. MR3588733

[8] D. A. Di Pietro and A. Ern, *Mathematical Aspects of Discontinuous Galerkin Methods*, Mathématiques & Applications (Berlin) [Mathematics & Applications], vol. 69, Springer, Heidelberg, 2012. MR2882148

[9] J. Diaz and M. J. Grote, *Energy conserving explicit local time stepping for second-order wave equations*, SIAM J. Sci. Comput. **31** (2009), no. 3, 1985–2014, DOI 10.1137/070709414. MR2516141

[10] J. Diaz and M. J. Grote, *Multi-level explicit local time-stepping methods for second-order wave equations*, Comput. Methods Appl. Mech. Engrg. **291** (2015), 240–265, DOI 10.1016/j.cma.2015.03.027. MR3345249

[11] R. Diehl, K. Busch, and J. Niegemann, *Comparison of low-storage Runge-Kutta schemes for discontinuous Galerkin time-domain simulations of Maxwell's equations*, J. Comput. Theor. Nanosci. **7** (2010), no. 8, 1572–1580.

[12] V. Dolean, H. Fahs, L. Fezoui, and S. Lanteri, *Locally implicit discontinuous Galerkin method for time domain electromagnetics*, J. Comput. Phys. **229** (2010), no. 2, 512–526, DOI 10.1016/j.jcp.2009.09.038. MR2565614

[13] M. Dumbser, M. Käser, and E. F. Toro, *An arbitrary high-order Discontinuous Galerkin method for elastic waves on unstructured meshes – V. Local time stepping and p-adaptivity*, Geophys. J. Int. **171** (2007), no. 2, 695–717.

[14] E. Emmrich, *Discrete versions of Gronwall's lemma and their application to the numerical analysis of parabolic problems*, Preprint no. 637, Fachbereich Mathematik, TU Berlin, 1999.

[15] M. J. Grote, M. Mehlin, and T. Mitkova, *Runge-Kutta-based explicit local time-stepping methods for wave propagation*, SIAM J. Sci. Comput. **37** (2015), no. 2, A747–A775, DOI 10.1137/140958293. MR3324978

[16] J. Diaz and M. J. Grote, *Energy conserving explicit local time stepping for second-order wave equations*, SIAM J. Sci. Comput. **31** (2009), no. 3, 1985–2014, DOI 10.1137/070709414. MR2516141

[17] M. J. Grote and T. Mitkova, *Explicit local time-stepping methods for Maxwell's equations*, J. Comput. Appl. Math. **234** (2010), no. 12, 3283–3302, DOI 10.1016/j.cam.2010.04.028. MR2665386

[18] M. J. Grote and T. Mitkova, *High-order explicit local time-stepping methods for damped wave equations*, J. Comput. Appl. Math. **239** (2013), 270–289, DOI 10.1016/j.cam.2012.09.046. MR2991972

[19] J. S. Hesthaven and T. Warburton, *Nodal high-order methods on unstructured grids. I. Time-domain solution of Maxwell's equations*, J. Comput. Phys. **181** (2002), no. 1, 186–221, DOI 10.1006/jcph.2002.7118. MR1925981

[20] J. S. Hesthaven and T. Warburton, *Nodal Discontinuous Galerkin Methods*, Texts in Applied Mathematics, vol. 54, Springer, New York, 2008. Algorithms, analysis, and applications. MR2372235

[21] M. Hochbruck and A. Ostermann, *Exponential multistep methods of Adams-type*, BIT **51** (2011), no. 4, 889–908, DOI 10.1007/s10543-011-0332-6. MR2855432

[22] M. Hochbruck and T. Pažur, *Implicit Runge-Kutta methods and discontinuous Galerkin discretizations for linear Maxwell's equations*, SIAM J. Numer. Anal. **53** (2015), no. 1, 485–507, DOI 10.1137/130944114. MR3313827

[23] M. Hochbruck, T. Pažur, A. Schulz, E. Thawinan, and C. Wieners, *Efficient time integration for discontinuous Galerkin approximations of linear wave equations*, ZAMM Z. Angew. Math. Mech. **95** (2015), no. 3, 237–259, DOI 10.1002/zamm.201300306. MR3324777

[24] M. Hochbruck and A. Sturm, *Error analysis of a second-order locally implicit method for linear Maxwell's equations*, SIAM J. Numer. Anal. **54** (2016), no. 5, 3167–3191, DOI 10.1137/15M1038037. MR3565552

[25] P. Monk, *Finite Element Methods for Maxwell's Equations*, Numerical Mathematics and Scientific Computation, Oxford University Press, New York, 2003. MR2059447

[26] E. Montseny, S. Pernet, X. Ferriéres, and G. Cohen, *Dissipative terms and local time-stepping improvements in a spatial high order discontinuous Galerkin scheme for the time-domain Maxwell's equations*, J. Comput. Phys. **227** (2008), no. 14, 6795–6820, DOI 10.1016/j.jcp.2008.03.032. MR2435431

[27] L. Moya, *Temporal convergence of a locally implicit discontinuous Galerkin method for Maxwell's equations*, ESAIM Math. Model. Numer. Anal. **46** (2012), no. 5, 1225–1246, DOI 10.1051/m2an/2012002. MR2916379

[28] F. Müller and C. Schwab, *Finite elements with mesh refinement for elastic wave propagation in polygons*, Math. Methods Appl. Sci. **39** (2016), no. 17, 5027–5042, DOI 10.1002/mma.3355. MR3573650

[29] A. Pazy, *Semigroups of Linear Operators and Applications to Partial Differential Equations*, Applied Mathematical Sciences, vol. 44, Springer-Verlag, New York, 1983. MR710486

[30] S. Piperno, *Symplectic local time-stepping in non-dissipative DGTD methods applied to wave propagation problems*, M2AN Math. Model. Numer. Anal. **40** (2006), no. 5, 815–841 (2007), DOI 10.1051/m2an:2006035. MR2293248

[31] A. Sturm, *Locally implicit time integration for linear Maxwell's equations*, Ph.D. dissertation, Karlsruhe Institute of Technology, 2017.

[32] J. G. Verwer, *Component splitting for semi-discrete Maxwell equations*, BIT **51** (2011), no. 2, 427–445, DOI 10.1007/s10543-010-0296-y. MR2806538

Institute for Applied and Numerical Analysis, Karlsruhe Institute of Technology, Kaiserstr. 12, 76131 Karlsruhe, Germany

Email address: marlis.hochbruck@kit.edu

Institute for Applied and Numerical Analysis, Karlsruhe Institute of Technology, Kaiserstr. 12, 76131 Karlsruhe, Germany

Email address: andreas.sturm@kit.edu